Bachelor thesis

Localization of a Radiation Source by a Formation of Unmanned Aerial Vehicles

Petr Štibinger

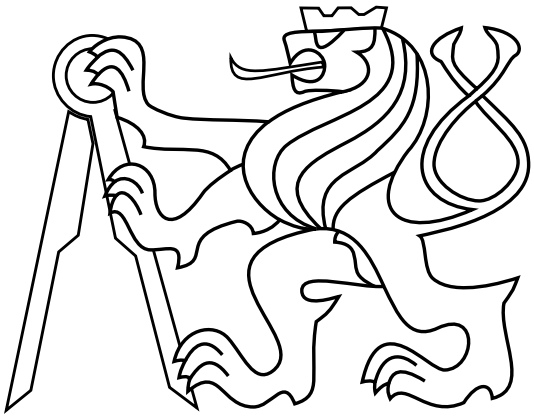

May 2017

Thesis supervisor: **Ing. Martin Saska, Dr. rer. nat.**

Czech Technical University in Prague
Faculty of Electrical Engineering, Department of Cybernetics

Declaration

I declare that the presented work was developed independently and that I have listed all sources of information used within it in accordance with the methodical instructions for observing the ethical principles in the preparation of university theses.

Prague, 25.5.2017

.....

Czech Technical University in Prague
Faculty of Electrical Engineering

Department of Cybernetics

BACHELOR PROJECT ASSIGNMENT

Student: Petr Š t i b i n g e r

Study programme: Cybernetics and Robotics

Specialisation: Robotics

Title of Bachelor Project: Localization of a Radiation Source by a Formation of Unmanned Aerial Vehicles

Guidelines:

The goal of the thesis is to design, implement in ROS (Robot Operating System), and experimentally verify in Gazebo simulator an algorithm for localization of sources of radiation by a formation of mutually localized unmanned aerial vehicles (UAV). The following tasks will be solved:

- To implement a model of Timepix detector being developed at UTEF CTU into the robotic Gazebo simulator based on the technical specification of the sensor and particle physics [1,2].
- To simulate a source of radiation in the Gazebo simulator (a simulation of decay of cesium - gamma and beta particles).
- To design a simple method for localization of the source by a single UAV using estimated direction of the source detected in the simulator.
- To design a simple strategy for localization of the source by a formation of UAVs and to study possibility of optimization of the formation shape with respect to maximal gained information.
- To prepare the system for experimental verification with the multi-UAV platform of the Multi-Robot Systems group [3] (the real experiment will be realized in future work based on availability of the Timepix detector).

Bibliography/Sources:

[1] Michal Platkevič. "Signal Processing and Data Read-Out from Position Sensitive Pixel Detectors". PhD thesis. Faculty of Nuclear Sciences and Physical Engineering, Czech Technical University in Prague, 2014.

[2] Zdeněk Vykydal. "Mikroprocesorem řízené rozhraní USB pro detektor Medipix2". Master thesis. Faculty of Nuclear Sciences and Physical Engineering, Czech Technical University in Prague, 2005.

[3] T. Baca, G. Loianno and M. Saska. Embedded Model Predictive Control of Unmanned Micro Aerial Vehicles. In 21st International Conference on Methods and Models in Automation and Robotics (MMAR). 2016.

[4] M. Saska, J. Langr and L. Preucil. Plume Tracking by a Self-stabilized Group of Micro Aerial Vehicles. In Modelling and Simulation for Autonomous Systems. 2014.

Bachelor Project Supervisor: Ing. Martin Saska, Dr. rer. nat.

Valid until: the end of the summer semester of academic year 2017/2018

L.S.

prof. Dr. Ing. Jan Kybic
Head of Department

prof. Ing. Pavel Ripka, CSc.
Dean

Prague, February 14, 2017

Acknowledgement

I would like to express gratitude to my thesis supervisor, Dr. Martin Saska, for his guidance and support throughout the last year, and the time and energy he invested into this work. I would also like to thank Ing. Tomáš Báča, who helped me understand the problematics and provided me with valuable advices. In addition, I would like to thank all the beautiful young women from my surroundings for their lack of interest in my person, which allowed me to dedicate all of my time to this thesis. Finally, my deepest gratitude goes out to my family for their continuous support throughout my studies and my through life in general.

Abstrakt

Tato práce se zabývá využitím skupin kooperujících bezpilotních helikoptér při vyhledávání zdrojů ionizujícího záření. Tento inovativní přístup je umožněn kombinací unikátního lehkého detektoru částic Timepix, na jehož vývoji se podílí také Ústav technické a experimentální fyziky ČVUT, a neméně unikátního systému pro stabilizaci skupin bezpilotních helikoptér, vyvíjeného ve skupině Multirobotických systému z Katedry kybernetiky na FEL ČVUT. Helikoptéry jsou osazeny těmito senzory a následně vyslány k aktivnímu vyhledávání neznámého zdroje ionizujícího záření. V rámci této práce byly navrženy dvě metody vyhledávání. První z těchto metod využívá pouze jednu helikoptéru, zatímco druhá zapojuje do hledání hned tři. Vzhledem k tomu, že v laboratorních prostorách nebylo možné rozmístit dostatek radioaktivního materiálu, bylo nutné na základě dostupných dat vytvořit simulační prostředí obsahující jak model zářiče, tak model částicového detektoru. Obě metody vyhledávání byly úspěšně vyzkoušeny jak v tomto simulátoru, tak také s použitím skutečných helikoptér výzkumné skupiny Multirobotických systémů.

Klíčová slova

Radioaktivita, ionizující záření, formace bezpilotních helikoptér, částicový detektor, Timepix, simulace, Unscented Kalman filter

Abstract

This thesis deals with cooperative use of multiple unmanned helicopters for localization of ionizing radiation sources. This novel approach was made possible by combining a unique, lightweight particle detector Timepix, and an equally unique system for stabilization of a group of unmanned helicopters developed by the Multi-Robot Systems research group at the Department of Cybernetics at FEE CTU. The Czech Technical University also contributes to the development of Timepix via the Institute of Experimental and Applied Physics. Helicopters are equipped with these detectors and used in an active searching for an unknown radiation source. Two methods for localization of the source were designed. The first approach is fairly simple and uses a single helicopter, while the second is much more complex and uses a formation of three helicopters. Since it was not possible to deploy the necessary ammounts of radioactive material in laboratories, a simulation enviroment was created with the use of avaliable data, to simulate a radiation source as well as the particle detector. Both localization methods were successfuly tested in this simulator and also with the use of real helicopters of the research group Multi-Robot Systems.

Keywords

Radioactivity, ionizing radiation, formation of unmanned helicopters, UAV, particle detector, Timepix, simulation, Unscented Kalman filter

Contents

Abbreviations

Abbreviations and symbols used in this thesis are listed here.

^{137}Ba - Barium-137
Bq - Becquerel, unit of activity
CERN - European Organization for Nuclear Research
^{137}Cs - Cesium-137
CTU - Czech Technical University
EKF - Extended Kalman Filter
FEE - Faculty of Electrical Engineering
IEAP - Institute of Experimental and Applied Physics
ID - Identification
ISS - International Space Station
keV - Kiloelectronvolt
MeV - Megaelectronvolt
MPC - Model Predictive Control
MRS - Multi-Robot Systems
NUC - Next Unit of Computing
N_A - Avogadro constant
NPP - Nuclear Power Plant
Q2 - Second quarter of a calendary year
RFID - Radio-frequency Identification
ROS - Robot Operating System
RTK - Real-Time Kinematics
SATRAM - Space Application of Timepix based Radiation Monitor
^{90}Sr - Strontium-90
$t_{1/2}$ - Half-life of a radioisotope
UAV - Unmanned Aerial Vehicle
UKF - Unscented Kalman Filter
USB - Universal Serial Bus

1 Introduction

In recent years, mobile devices have experienced a rapid growth. Smartphones and tablets can now possess the computing power of a desktop computer. These advancements have also spread into the field of mobile robotics. Unamnned aerial vehicles (UAVs) have become avaliable and affordable for almost anyone. They are capable of performing complex tasks and staying in the air for more than 20 minutes. Based on equipped hardware, UAVs can be used in various ways including aerial footage, surveillance, package delivery, drone racing, search and rescue operations and many more.

In the last couple of decades, mankind has also learned to harness the power of nuclear fission. It has become the most powerful source of energy, which can be held under control. This kind of power generation, however, both requires and produces radioactive materials. All these materials share a specific property - they emit ionizing radiation. This radiation damages living tissue, but a human body cannot sense it on its own. Specialized detectors are therefore required.

One such device is the Timepix, a detector developed at CERN[1] in collaboration with the IEAP CTU[2] [1], [2], [3], [4]. The Timepix consists of a semiconductor chip with a resolution of 256×256 pixels at a size of just 1.4×1.4 cm^2, and readout electronics, which varies in size based on the configuration. In the most compact version called USB Lite, the device is as small as a USB flash drive. This device is shown in Figure 2. These detectors have already found a wide array of applications, ranging from X-ray tomography or non-destructive material analysis up to detection of cosmic ray bursts.

This thesis focuses on using particle detectors onboard UAVs to find sources of ionising radiation. UAVs provide reliable movement over difficult terrain and the option to explore extremely polluted and hazardous areas, that would require several layers of protective clothing when visited personally. This makes UAVs suitable for surveying in sites of a nuclear disaster (Chernobyl, Fukushima) or radioactive material deposits such as Uranium ore mines or nuclear waste storage. Besides the contaminated areas, strong sources of radiation can also appear in populated areas, for example as an act of terrorism. Localization of a radiation source in an urban area is done by ground-based measurements using hand-held detectors or specialized vehicles, such as trucks equipped with large radiation detectors, or piloted aircrafts [5]. UAVs carrying Timepix detectors are expected to provide more flexibility when performing the same task.

Since this work is a first step of research in the field of UAVs at CTU in Prague dealing with radiation, one of the goals of this thesis is to create the necessary simulation enviroment, where localization approaches can be designed and tested. This way, the approaches can be verified without the need to travel into radiation-polluted areas or to replicate similar conditions in laboratory areas, which is costly and time-consuming with all the necessary safety precautions.

The localization relies on the ability to determine a direction of incomming particles. This can be achieved by rotating the sensor and observing the difference in measurements (explained later in Section 5.1). More sophisticated approach would require multiple Timepix chips on every helicopter, or a specialized coating for the detection

[1] Conseil Européen pour la Recherche Nucléaire - The European Organization for Nuclear Research
[2] Institute of Experimental and Applied Physics of the Czech Technical University in Prague

surface, which would provide the ability to measure the direction directly. These additions would significantly speed up the detection process and are planned for use in future work. Data measured by the Timepix in combination with a known position of the UAV can be used to calculate the position of the source. Two different approaches were designed and tested as a part of this thesis. A solo approach using one UAV equipped with a single detector, and a cooperative approach using a formation of three relatively localized UAVs, each equipped with its own detector. Both of the approaches have been implemented and experimentally verified in a robotics simulator Gazebo [6]. In addition, these approaches have been used to navigate a group of real stabilized helicopters. These real experiments have been made possible by using the model of a radioactive source described in this thesis. A snapshot from these experiments, with a formation of UAVs hovering above the radiation source can be seen in Figure 1.

1.1 State of the art

Detection of high-energy ionizing particles is an important part of astronomy. By locating the origin of incomming cosmic rays, astronomers are able to track supernovae, black holes and other astronomical objects of extreme energy. Largest such device currently deployed in Earth's orbit is the Fermi Gamma-ray space telescope [7]. This telescope uses a scintillation detector - large crystal of a transparent material (e.g. Sodium Iodide), which emits photons (flashes in visible light or ultraviolet spectrum), when a charged particle passes through the crystalline structure. These flashes are then analyzed by a specialized electronics to determine properies of the particle. Because of a large number of components, high price and power consumption, scintillation detectors are inappropriate for use onboard UAVs or small spacecrafts.

The Timepix, on the other hand, is a lightweight and compact detector, making it more suitable for cubesats or small satellites in general. It has been successfully used in the SATRAM[3] module [8], which was launched into low Earth orbit in 2013 onboard the European satellite PROBA-V. Additional spacecrafts equipped with Timepix or related detectors include the Japanese RISESat [4] (multiple delays, launch date not specified) or the VZLUSAT-1 [9] (scheduled for launch in Q2 2017). Six detectors have been mounted onboard the ISS[4] since 2012 [10].

Various robotic projects also keep track of radiation here on our planet. Following the Fukushima-Daiichi nuclear power plant disaster in 2011, the contaminated area has been under surveillance of unmanned aircrafts. Off-the-shelf UAVs are used to survey smaller areas from lower altitudes [11], [12] and large military drones are used to map the entire exclusion zone [13]. Various other applications using UAVs for radiation detection have been proposed. These applications include measuring levels of airborne radioactive fallout [14], cooperative contouring of an irradiated area [15] or radiation level surveying along pre-defined trajectories [16].

In addition to the research on radiation detectors, this thesis benefits of a long term research on formation flying [17], [18], [19], [20], [21], [22] and stabilization of compact swarms of UAVs [23], [24] conducted at the Multi-Robot systems group of CTU in Prague. The aim of this thesis is to apply these general methods of control of UAV groups in this unique application and to use the flexibility of formations (possibility to change shape and position) to increase precision of the localization in a way similar to searching for RFID transmitters [25], surveillance scenarios [26], [27], [28], maritime

[3]The Space Application of Timepix based Radiation Monitor
[4]International Space Station

distress beacon localization [29] or plume detection [30].

All previously mentioned projects consider the radioactive material to be spread over a large perimeter. This thesis deals with searching for a single strong source in an otherwise "clean" area. A similar research, focused at detection of incomming particle direction with an innovative detector called the Radiation Compass [31], is being conducted at the Oregon State University. However, to our best knowledge, this task has never been solved by a group of cooperating helicopters before.

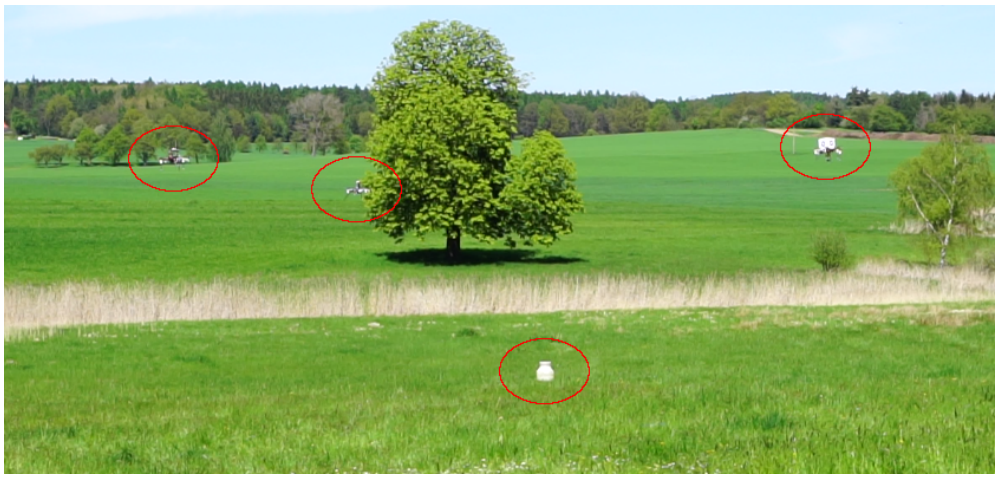

Figure 1 A formation of three UAVs searching for a radiation source (white barrel). No radioactive material has been used during the real experiments, the radioactive particles have been simulated. The barrel was only used to visually mark the position of the source.

Figure 2 Particle detector Timepix in the smallest variant USB Lite. The Silicon detector chip can be seen on the left (silver surface), the readout electronics is covered by a plastic casing. It is worth noting, that the size of the Silicon chip is the same for all variants at 1.4×1.4 cm. Source: `http://aladdin.utef.cvut.cz/utef_web_pictures/anniversary/tpx_usb_lite_small.jpg`

2 Problem definition

This thesis deals with a different problem than related work with UAVs focused around radioactivity. As mentioned in Section 1.1, the operational area will contain only a single strong source of radiation. The goal is to navigate and optimally distribute the UAVs in such way, that the radiation source is localized with the highest accuracy. UAVs will operate autonomously without any previous information about the source, using only data from onboard sensors.

This project requires the UAVs to be relatively localized and to communicate via a wireless technology. The relative position of the UAVs can be obtained either from a satellite navigation system (GPS, Galileo, GLONASS, BeiDou...) or an onboard relative localization system [32], [33].

Size and shape of the area of operation is known beforehand. A single source of radiation is placed in this area. There are no obstacles to be avoided and particles emitted by the source are only blocked by air. The avaliable data on particle behaviour consider the air to be dry and at standart laboratory pressure[1]. Therefore, the air is considered to possess the same properties in all scenarios described in this thesis. For simplicity, the UAVs move in a fixed altitude.

2.1 Contributions

Models of radioactive Cesium-137 and the Timepix detector have been implemented for use in the simulator Gazebo (further described in Section 3.4). Furthermore, two different localization approaches have been designed and implemented - a simple solo approach using one UAV, and a cooperative approach using a formation of three UAVs. The solo approach is further described in Section 5.2 and the cooperative one in Section 5.3. Both methods have been experimentally verified in the simulator Gazebo and also tested on a platform of the Multi-Robot Systems (MRS) group at FEE CTU[2] using real, relatively localized UAVs [34]. Both Timepix and Cesium were simulated during the real experiments with the use of previously mentioned models. Simulation results and findings are presented in Sections 6.1 and 6.2, for one and three UAVs respectively. Real experiments along with results are described in Chapter 7. Evaluation of the results and comparison of the two approaches, as well as comparison of the real and simulated platform, are presented in Chapter 8.

[1] 1 atm = 101 325 Pa

[2] Faculty of Electrical Engineering, Czech Technical University

2.2 System description

The system consists of one or three UAVs searching for a single radiation source. Following assumptions are considered:

The radiation source is simplified to a point source. It does not move or change its properties during the experiment. Activity[3] and position of the source is previously unknown to the control system used by the UAVs. The source emits particles randomly and their spatial distribution is uniform. The trajectory of every particle is a straight line. Both beta and gamma particles are emitted at velocities highly superceeding the maximal speed of UAVs. Time of flight of the particles is therefore omitted.

Each UAV is equipped with one simulated Timepix detector. The detector is attached to the top of UAVs as shown in Figure 3. This way, center of the UAV and center of the detector will have the same global coordinates [X,Y]. Yaw (rotation around Z axis) will have significantly higher impact on the ammount of detected particles than roll and pitch, as the measurement is done with the UAV hovering in one place or moving very slowly (futher explained in Section 5.1). Both roll and pitch are therefore not considered in the calculations.

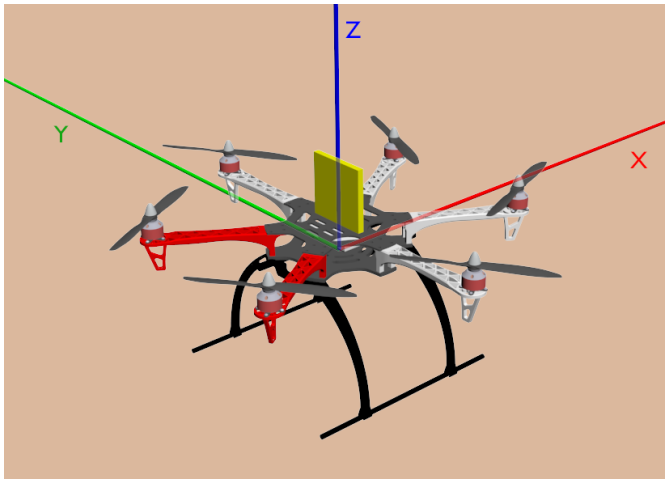

Figure 3 Detector (represented by a yellow box, size exaggerated) is attached to the top of a UAV in YZ plane, centered along the Z axis. This way, global coordinates [X, Y, yaw] of the UAV can also be used for the detector without further transformations.

[3]Number of emissions per second

3 Preliminaries

3.1 Radioactivity

Radioactivity, or radioactive decay, is a naturally occuring process by which an unstable atom loses its energy by emitting radiation. The radiation can be emitted in form of alpha particles, beta particles or gamma rays. The decay is a stochastic (random) process. For a single atom, neither time or direction of the emission can be predicted. However, certain properties can be used to describe a collection of these atoms. Such properties include half-life and activity.

Half-life describes a time interval, during which one half of atoms undergoes the decay process. In other words, every atom has a 50% probability of decaying during this time. Half-life of atoms can range from only a few nanoseconds to hundreds of years.

Activity describes an average number of decays per second. Unit of activity is becquerel (Bq) and 1 Bq is equal to 1 decay per 1 second. This property is very useful for simulation since it can provide frequency for the radiation source model. Activity of an isotope can be calculated using the following equation

$$A = \frac{m}{m_a} N_A \frac{ln(2)}{t_{1/2}}, \tag{1}$$

where m is mass of the sample, m_a is mass of one atom of the isotope, $N_A \approx 6.022 \cdot 10^{23}\,\mathrm{mol}^{-1}$ is the Avogadro constant (number of atoms in one mole) and $t_{1/2}$ is half-life of the isotope.

3.1.1 Radiation types

Alpha particles are nuclei of Helium, consisting of two protons and two neutrons. Of all radiation types, alpha particles are the least dangerous. They can be easily stopped by reaction with other matter because of their high mass and positive charge. Sufficient shielding is provided by a single sheet of paper or a few centimeters of air.

Beta particles are free electrons or positrons (anti-electrons) of high speed and energy. They have lower mass and less charge than alpha particles, thus they can penetrate thicker materials. Beta particles can be usually stopped by a few milimeters of aluminium. This is, however, not considered sufficient shielding, because a beta particle moving through matter can generate gamma rays through electromagnetic interactions.

Gamma rays are a form of electromagnetic radiation (photons) of very high energy and short wavelength. No border wavelength between X-rays and gamma rays is defined, therefore some very hard X-rays can possess higher energy than gamma rays. In related work, all photons produced by radioactive decay are usually classified as gamma rays regardless of their energy. This classification will be used in this thesis as well. Beacuse of their lack of mass and charge, gamma rays are very difficult to stop. Shielding is usually done by several centimeters of lead.

All three types of radiation have damaging effects on human body. They can cause skin burns, damage cell reproduction (which leads to cancer), or trigger mutations in DNA.

3.1.2 Dangerous isotopes

There are many radioactive isotopes, which are potentially dangerous for people and other living creatures. Some radioactive materials, such as Uranium or Radon, occur naturally. Others are created artificially for a specific purpose, or as a waste product of nuclear fission. Two of the most persistent ones are Cesium-137 (^{137}Cs) and Strontium-90 (^{90}Sr). Both of these isotopes are created as secondary products of Uranium-235 nuclear fission, which is the main source of power for many nuclear power plants and nuclear weapons.

Both ^{137}Cs and ^{90}Sr have a half-life of around 30 years. Thus, areas polluted by these isotopes remain contaminated over a very long timespan. Cesium is easily soluble in water but does not seem to accumulate in human body. Its natural decay however emits gamma rays. Strontium, on the other hand, only emits beta particles, but human body treats it the same way as Calcium and stores it in bones.

3.1.3 Cesium-137

For the purpose of this work, ^{137}Cs was chosen, because it emits gamma rays and thus can be detected from a greater distance than ^{90}Sr. Decay chain of ^{137}Cs is shown in Figure 4. Each atom has a 94.6% probability of decaying into metastable Barium-137(m) by emission of a 512 keV beta particle. Half-life of ^{137}Ba(m) is 2.55 minutes and then it transforms into stable ^{137}Ba by emission of 661.7 keV gamma ray. The remaining 5.4% is probability of transforming directly into stable ^{137}Ba by emitting a 1.174 MeV beta particle. Since no other decay chain produces ^{137}Ba(m), peak in gamma spectrum around 661.7 keV can be used to determine presence of ^{137}Cs .

The dominance of ^{137}Cs in nuclear fallout can be seen in Figure 5, which shows a spectrum of gamma radiation measured near Chernobyl NPP[1] 25 years after the disaster. The spectrum displays a very prominent peak caused by presence of ^{137}Cs .

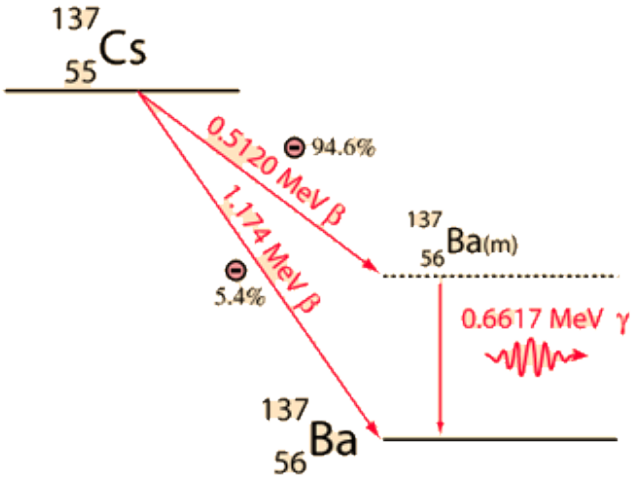

Figure 4 Decay chain of Cesium-137 showing two possible products. Majority of atoms emits beta particle while transforming into metastable Barium-137(m), which then emits gamma rays and transforms into stable Barium-137. Small ammount of atoms decays directly into stable ^{137}Ba by emission of a highly energetic beta particle. Source: `http://hyperphysics.phy-astr.gsu.edu/hbase/NucEne/imgnuk/cs137decay.gif`

[1] Nuclear power plant

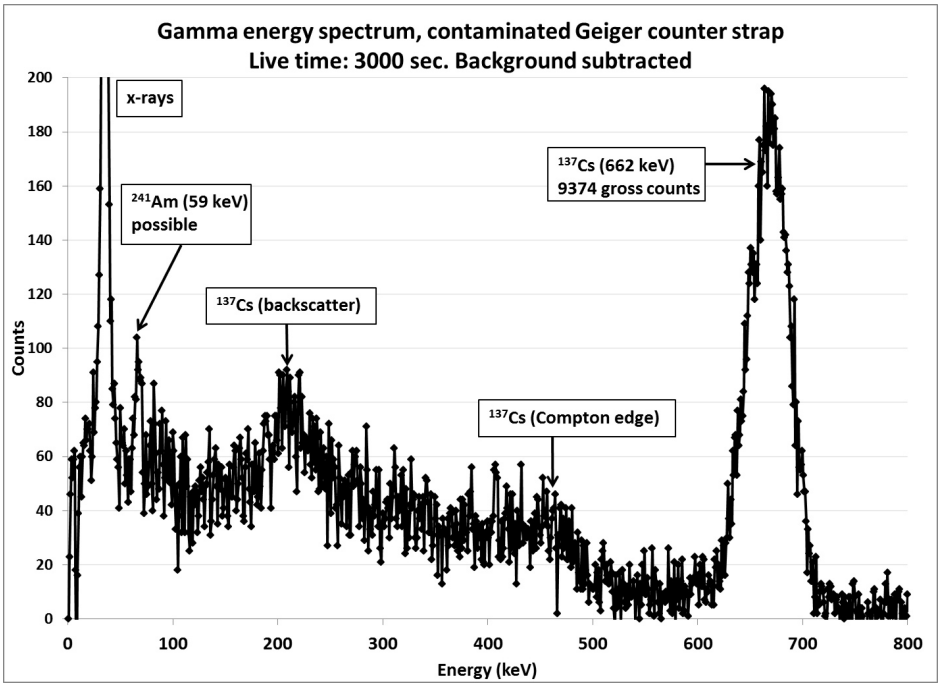

Figure 5 Spectrum of gamma rays measured in contaminated area surrounding the Chernobyl nuclear power plant. The spectrum shows most prominent peak around energy of 662 keV, which is released as a secondary product of Cesium-137 decay. Source: `http://carlwillis.files.wordpress.com/2011/03/chernobyl_strap_spectrum.jpg`

3.2 Timepix detector

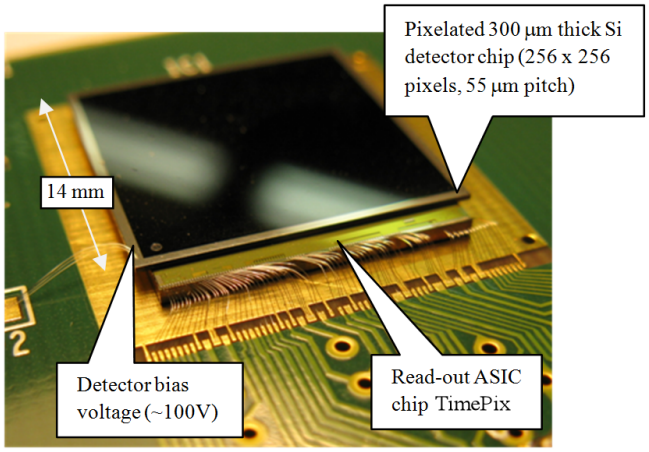

Figure 6 Pixel detector Timepix. *"Device consists of two chips connected by bump-bonding technique. The upper chip is pixelated semiconductor detector (usually Silicon). The bottom chip is ASIC read-out containing matrix of 256 × 256 of preamplifiers comparators and counters."* Official description taken from [35].

For this project, the hybrid[2] pixel detector Timepix was selected. This state of the art detector is a technological successor to sensors Medipix and Medipix2. These detectors have been developed by scientists from CERN in collaboration with other European

[2]Hybrid detector - the sensoric part and readout part are manufactured separately

institutions, most notably the Institute of Experimental and Applied Physics of the Czech Technical University in Prague [36].

These detectors have already been used in a wide range of applications such as high resolution X-ray imaging [37], non-destructive painted art analysis [38], cosmic radiation monitoring onboard the ISS[3] [10] or as a space telescope operating in X-ray and gamma energy spectrum [4] and [9]. Detailed description of the detector and principles of particle detection, as well as an in-depth breakdown of the various radiation types, can be found in [4]. Information regarding the readout part of the chip and a USB interface (suitable for use onboard the UAV platform) can be found in [2].

The detector has an active area of 14.08×14.08 mm consisting of 256×256 pixels. The detector is capable of operating at frequencies up to 100 kHz and overflows at 11810 particles per cycle [36]. It can be used in three different modes:

- Medipix mode - works as a precise particle counter with a given readout frequency.
- Time over threshold mode - works as an energy sensitive detector. Each incomming particle changes charge of impacted pixel. Time needed to restore original charge is then used to determine the particle energy.
- Timepix mode - works as an incidence timer. It allows measurement of the exact time of each particle hit.

In the smallest configuration is size of an entire device reduced to 15 mm $\times$ 60 mm (including the detector, readout electronics and interface connectivity). This version is called *USB Lite* and uses USB 1.0 for communication and powering the device. Due to its small size, low power consumption and common interface, it is suitable for use onboard a UAV.

The detectors can also be stacked as shown in Figure 7 to extend the detection capability into 3D. Detectors in this configuration are capable of detecting energy and direction of incomming particles at the same time. This is accomplished by searching for matching patterns in measurements from every layer [39].

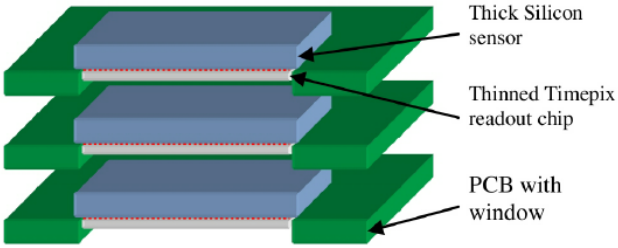

Figure 7 Stack of three Timepix detectors creating a 3D sensitive voxel detector. This stacking adds directional sensitivity and better noise suppression [39].

This kind of stacked detector would significantly improve the localization performance. At the moment, however, the device produces a lot of heat and requires water cooling. This may change in the future, as the device undergoes more development. Until then, a single-chip detector for each UAV will have to suffice.

[3] International Space Station
[4] Voxel is a 3D counterpart of pixel

3.3 Robot Operating System

The Robot Operating System (ROS) is a free, complex framework for creation of robotics software. It is developed by the Open Source Robotics Foundation[4]. It features various tools and libraries aimed to simplify creation of complex robotic systems. The software can be implemented in either C++, Python or LISP and there are also various extensions allowing the use of other programming languages, such as Java or JavaScript. The framework can also be used along with MATLAB, as both parties provide libraries for easy integration. With the right configuration, ROS can used to execute MATLAB code and results can be logged and evaluated in MATLAB. More details, as well as tutorials on how to use ROS, are avaliable online at the online ROS Wiki[5] [40].

Each software component in ROS is represented by a package. Each package has to contain a source code, a makefile with instructions for compilation and a package description. Other files are optional. These include launchfiles for running the package with parameters or additional libraries needed for the package to work correctly.

Core parts of ROS, such as the communications infrastructure, define some basic conventions for all packages. By following these conventions, each additional package can be created without the need to worry about compatibility with existing packages. The UAV platform of the Multi-Robot Systems group has also been created with ROS, thus it could have been easily extended with the results of this thesis.

3.3.1 ROS infrastructure

Upon executing a package code, a new **node** is created. Each node has its unique **ID** and is destroyed after it had finished all tasks or a new node with the same ID had been created. One of the core components in ROS is passing **messages** between nodes. This is done by a **Publisher-Subscriber** architecture, where a publisher node creates a **topic** (or uses an existing one) and all nodes subscribed to this topic recieve its messages. One topic can be both published into and subscribed by multiple nodes.

3.4 Gazebo simulator

Gazebo is a free robotics simulator also developed by the Open Source Robotics Foundation. It offers full integration of ROS, allowing the user to run ROS nodes in a simulated enviroment with realistic physics, 3D graphics visualisation and pre-built components commonly used in robotics (e.g. sensors or cameras).

The simulator has a built-in set of primitive objects (box, sphere, cylinder) and objects created in a third-party 3D modelling program can be imported. Rendering is done using the open-source engine OGRE[6]. The default physics engine is ODE with an option to download and use another engine (Bullet, Dart or Simbody) [6].

[4] `https://www.osrfoundation.org/`
[5] `http://wiki.ros.org/`
[6] `http://www.ogre3d.org/`

4 Gazebo model

This chapter describes all new ROS nodes created for purpose of this work, and should serve as a guide on how to use them. Both radiation source and Timepix models are intended for use in the simulator Gazebo, but can be used on the real UAV platform as well. Because of that, an experiment with real UAVs was made possible, even though the Timepix detector and radioactive material were not avaliable.

Figure 8 shows how are all the used nodes connected. Source node publishes particles to all Timepix nodes. The detector recieves position and rotation of the UAV from Odometry node and publishes measured radiation intensity to the Estimation node. The estimator uses odometric data and measured intensity to determine new position for each UAV. This position is then messaged to node Model Predictive Control (MPC), which handles the flight trajectory. Odometry and MPC nodes are already existing components of the MRS platform.

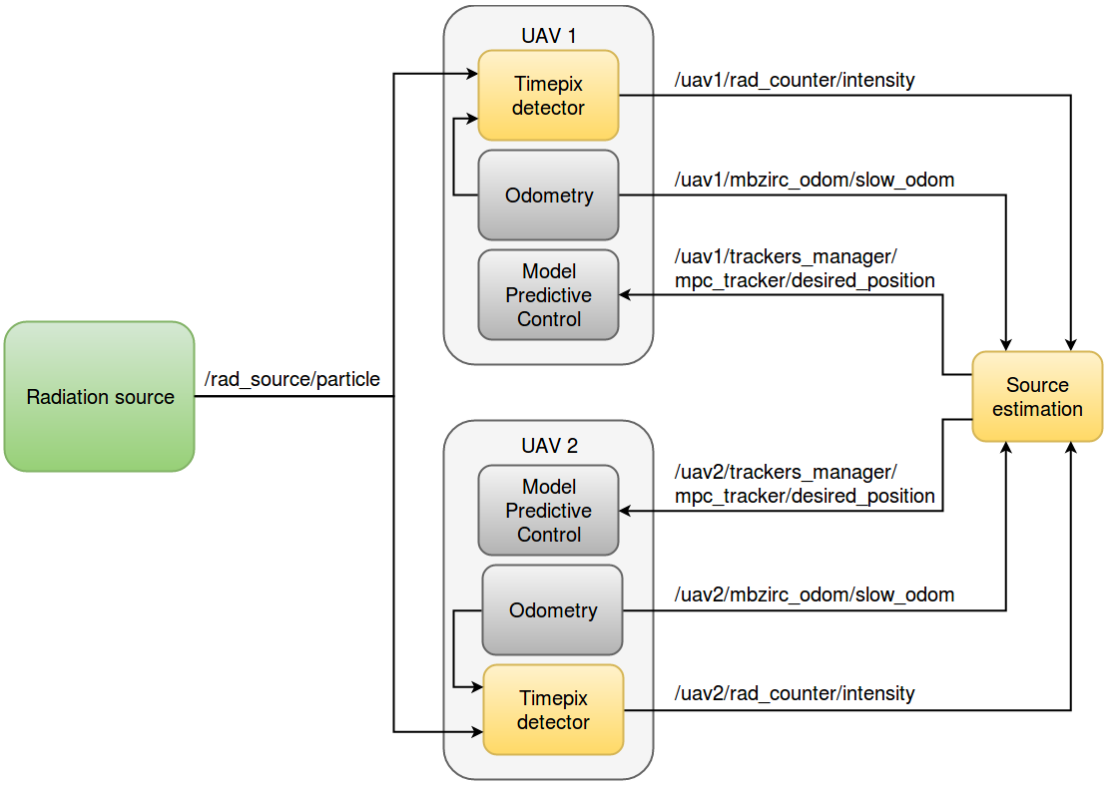

Figure 8 Diagram showing communication between individual ROS nodes (blocks) with used topics (arrows, orientation denotes which node is publisher and which is subscriber). Cooperative localization uses this exact communication with 3 UAVs (only 2 shown here for simplicity). Grey blocks are existing nodes of the Multi-Robot Systems group platform.

4.1 Radiation source

Radioactivity is a stochastic process, since both direction and emission time of every particle is random, as described in Section 3.1. However, for large ammount of atoms, activity can be determined as described by Equation 1. Activity can be represented as an average emission frequency of the source, which is very useful for the simulation. Real activity, however, is often extremely large number and such frequency cannot be simulated. For example, one gramm of ^{137}Cs has an activity of 3.215×10^{12} Bq which would require a frequency of 3.215 THz[1].

To overcome this problem, the frequency needs to be lowered and scale of the detector increased. Number of particles hitting the detector in a given timespan is required to remain the same. The scaling is described by following equation

$$S = \sqrt{\frac{A}{f}}, \tag{2}$$

where S is scaling constant for model of detector surface, A is real activity of the source and f is frequency of the computer model. A scaling constant for one side of the detector is then calculated as $\sqrt{S}$.

For the model of Cesium, gamma and beta particles are simulated. The decay chain on Figure 4 shows two possible products. The outcome is chosen randomly in each cycle with respect to given probabilities. Because of a huge difference between half-life of Cesium-137 and Barium-137m (30 years $\gg$ 153 seconds), gamma rays are emitted immediately after the initial beta emission.

The radiation source has been implemented as a ROS node operating at a high frequency (1 MHz by default). In each cycle, the node publishes a custom message called **particle**. Data stored in this message are described in Table 1. These messages are published to a topic called `/rad_source/particle`.

Name	Format	Description
Type	`string`	Type of radiation (gamma or beta)
Energy	`float`	Energy of the particle in keV
Vec	3×`float`	X,Y,Z components of the particle's direction vector
Pos	3×`float`	X,Y,Z coordinates of the particle's origin
Scale	`float`	Scaling constant for one side of the detector

Table 1 Table of variables stored in a custom ROS message **particle**, that has been created to publish all the necessary data in one file.

As mentioned in Section 2.2, all particles move in straight lines. To describe a line in 3D, a point and a direction is required. The message also contains information about the type of radiation (gamma or beta) and energy of the particle. The last variable is a scaling constant for one side of the detector.

External configuration file is used, allowing changes of some properties without the need for compilation. These properties are: **mass** of the radioactive material, **position** in global coordinates, **frequency** of the model, half-life of the material and isotope mass. Chaning the half-life and isotope mass would most likely require some minor changes in the source code as well, because the decay chain may be different.

The model is also prepared to simulate multiple sources at the same time, each in different position and with different intensity.

[1] Required frequency is exceeding capabilities of current computers by three orders.

4.2 Detector

The detector surface is a square - part of a plane with given borders. To describe a plane in 3D, one point and a normal vector is needed. Yaw of the UAV is used to easily calculate the normal vector, since it is the *forward* direction of the helicopter. Position of the detector's center is derived from position of the UAV. Coordinates recieved from the Odometry node are moved by a given ammount in all three axes to get coordinates of the detector's center. This offset is a parameter and can be easily modified. **Offset** used for **all experiments** done in this thesis is $(0.0, 0.0, 0.1)$ meters, corresponding with the illustration shown on Figure 3.

Particle hits are solved as an intersection of a line and a plane. The process is described as Algorithm 1.

Algorithm 1 Detector model

```
1: Line l, Plane p
2: if (p||l) then
3:     return No hit
4: else
5:     Calculate Point H = p ∩ l
6:     if H lies outside the detector area then
7:         return No hit
8:     else
9:         Calculate distance the particle has travelled
10:        Determine a probability of the particle reaching the detector
11:        Roll a random number from interval < 0 ; 100 >
12:        if Random number > probability then
13:            return No hit
14:        else
15:            return Hit
16:        end if
17:    end if
18: end if
```

Probability of a particle reaching the detector depends on type and energy of the particle as well as the distance between the source and the detector. Figure 9 shows the range[2] of beta particles in dry air depending on their initial energy. Decay of ^{137}Cs emits beta particles at 541 keV with range of 1.6 m and 1176 keV with range of 4 m. Considering that the UAV will move in an altitude of 3 or more meters above the ground (and above the source), beta particles will be detected only if the UAV is extremely close to the source. Nevertheless, they are still simulated.

Gamma particles can reach much further. This can be seen in Figure 10, which shows a probability of a gamma ray reaching the corresponding distance. This dependency is described by Equation 3. This formula was derived from data publicly avaliable online at [41].

$$P(\%) = 100e^{-9.2387 \cdot 10^{-3} d} \tag{3}$$

In this equation, $P(\%)$ is a probability of a particle reaching a detector, d is the distance between a source and the detector in meters and e is the Euler's number.

[2]Range is a maximal distance the particle can travel before being absorbed

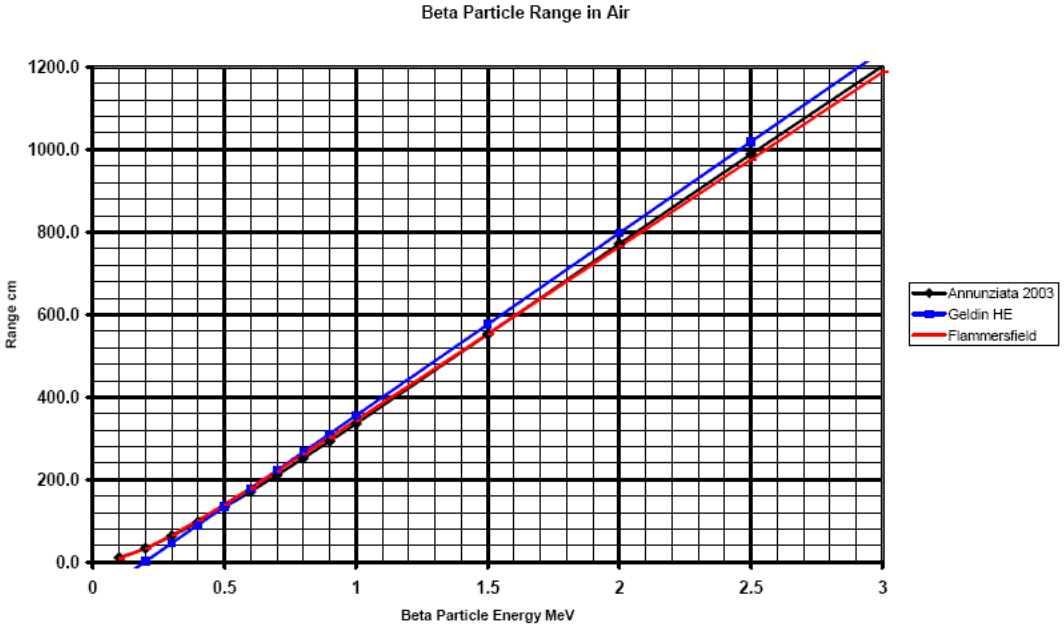

Figure 9 Range (maximal travel distance) of a beta particles in dry air depending on its initial energy. For beta particles released by ^{137}Cs decay, the range equals to 4 m at 1176 keV and 1.6 m at 541 keV. Source: `http://www.alpharubicon.com/basicnbc/images/article16radiological7102.gif`

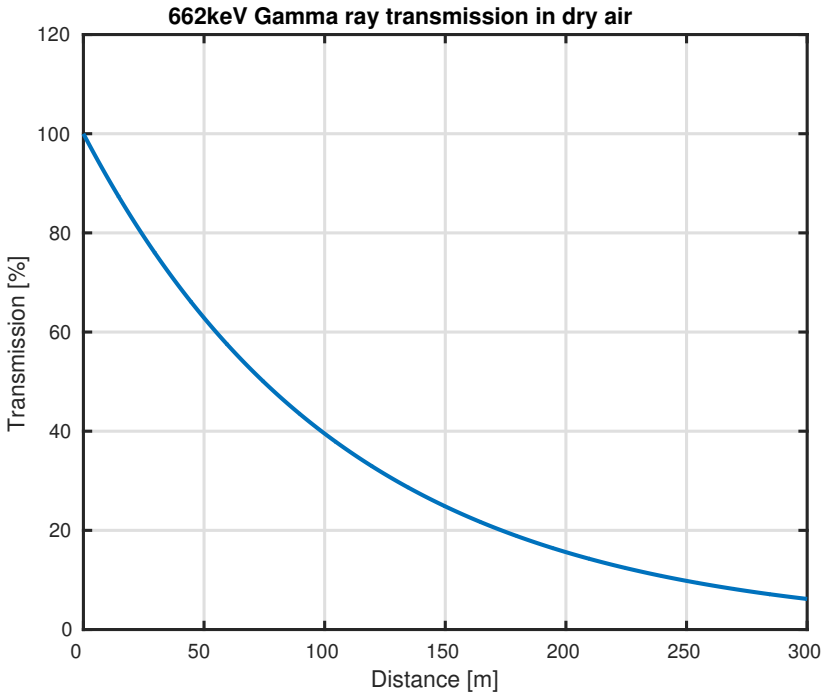

Figure 10 Transmission percentage of 662 keV gamma particles in dry air depending on distance. This curve is a plot of Equation 3 and is used to determine, whether a gamma particle was absorbed by air before reaching detector surface, or not.

The node counts particle hits per second, emulating the behaviour of Timepix in Medipix mode. Data measured by the sensor are published to the topic `/.../rad_counter/intensity` with the blank space being replaced by the name of a UAV carrying this detector. These topics are subscribed by an estimator node, which uses the intensity measurements to determine position of the source. This process is described later in Sections 5.2 and 5.3.

The model counts all particles that successfully reach the surface, whether they hit the front or the back side. This part will require some future tests with a real Timepix and a real radiation source, because the measurements might be affected by casing of the detector or some other factors.

5 Localization of radiation source

This chapter describes two approaches to localize a radioactive source by using autonomous UAVs. Both approaches utilize the ability to determine direction of incomming particles. This is done by combining intensity measurement from Timepix and odometry data from the UAV, more specifically the yaw (rotation around Z axis).

A single detector is mounted on top of the UAV, perpendicular to the ground (see Figure 3). The basic motivation is to change the yaw of the helicopter and count particles that hit the detector in a constant time window. The count is expected to be the highest, when the detector surface is pointed directly towards the source (see Figure 11). Since a single measurement provides a direction but not a distance, measurements have to be done in two different places, to estimate position of the source. This position is calculated as an intersection of two lines.

5.1 Direction estimation

Before a searching strategy could be implemented, the behaviour of the model had had to be tested. The UAV took k measurements, counted the total sum of detected particles, and then rotated by θ radians. The measurements were done for yaw in interval $< -\pi, \pi >$ (one full rotation).

The UAV was placed in position $(0.0, 0.0, 5.0)$ and measurement parameters were set to $k = 5$ s and $\theta = \frac{\pi}{20}$ rad. This rotation step was chosen, because it is the smallest yaw difference the controller of a real UAV can certainly provide. Multiple samples are taken in one direction to slightly reduce the randomness in measurements.

It is worth noting, that the source was placed in the same height as the UAV, to remove all other influences, and truly test only the dependence on yaw. This is the only case of the source not being placed on the ground (Z = 0) in the entire thesis.

Measurements were done with the source placed in positions $(0.0, 2.0, 5.1)$, $(0.0, 5.0, 5.1)$, $(0.0, 20.0, 5.1)$ and $(0.0, 50.0, 5.1)$[1]. Measured particle count is shown in Figures 12 and 13.

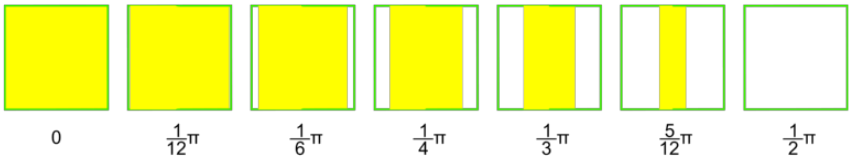

Figure 11 Actual (green) and apparent detector size (yellow), as seen from position of the source. Displayed numbers represent angle between particle direction and normal of the detector

[1]Used coordinates (X,Y,Z) and rotation of the UAV are related to the global coordinate system of the simulator Gazebo.

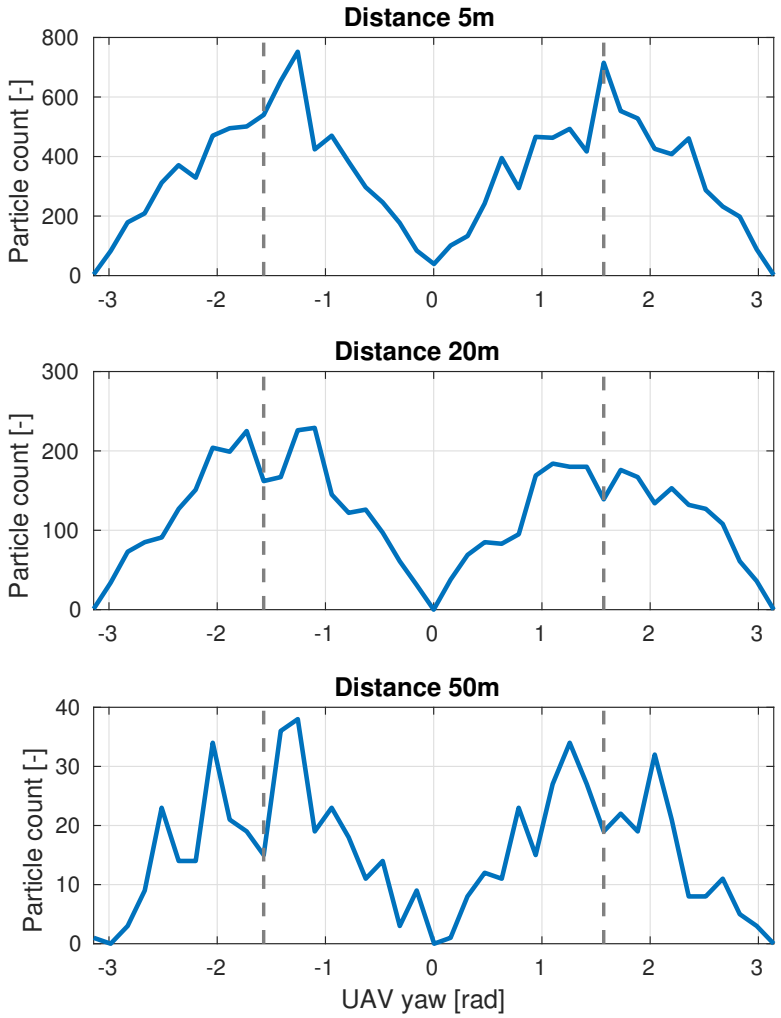

Figure 12 Particles detected from 5, 20 and 50 meters, while the UAV was changing yaw. The source was placed in the same height as the detector's center. Particles were counted for 5 seconds and rotation step was $\frac{\pi}{20}$ radians. The source was represented by 5 gramms of ^{137}Cs and the detector was facing directly towards the source at $-\frac{\pi}{2}$ and $\frac{\pi}{2}$ radians (marked by grey vertical lines). It is clear, that particle count is not guaranteed to peak at these values. The lowest values, on the other hand, are consistently located in the correct place (0 and $\pm\pi$ radians in this case).

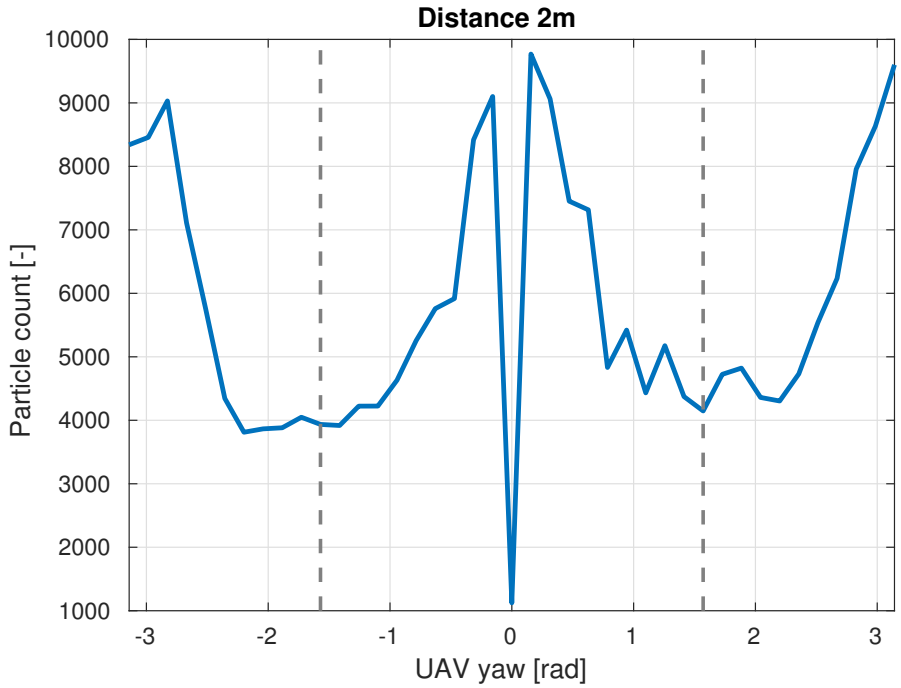

Figure 13 Particles detected from 2 meters, while the UAV was changing yaw.
For small distances, the model is no longer working as intended. To simulate 5 gramms of ^{137}Cs , the detector needs to be scaled to 4.36×4.36 meters. This causes the source to appear *inside* the detector at some point, creating additional spikes in intensity.

The measured radiation intensity is inversely proportional to the square of distance. Moreover, the stochastic nature of the source causes measurements to be more inaccurate with increasing distance, as the particle count gets lower. The highest count should occur when the detector surface is pointed directly towards the source (dashed vertical lines). However, this kind of direction estimation is not applicable because of inconsistencies, which can be seen in Figure 12. Using the lowest measured intensity, on the other hand, proved to be very accurate. The best direction can then be calculated as the worst direction rotated by $\frac{\pi}{2}$.

For a very small distance between the source and detector, the model stops working as intented. As explained before, size of the detector needs to be increased to compensate for lower frequency. If the distance is smaller than size of the detector, the source can actually appear *inside* the detector, causing additional intensity spikes at unexpected angles. This unwanted behaviour of the model is completely negated by both of the localisation algorithms, which will be shown later in this chapter.

The detector treats both sides of the detector as equally capable of detecting incomming radiation. This can be seen in Figure 12, where the plot is nearly symmetrical. Therefore, the simulation time can be cut in half by only taking measurements for yaw in interval $< 0; \pi)$ radians.

5.2 Single UAV

The goal of this section is to design a simple algorithm to find the radiation source with a single UAV and only one detector. Symbols and variables used in this section are listed in Table 2.

Symbol	Description
$\vec{S}$	Global coordinates [X,Y] of the source
h	Altitude of the UAV
d	2D distance between UAV and source
g	Distance between measure points
k	Number of samples
θ	Yaw step size
n	Number of steps ($\theta = \pi/n$)
$\vec{w}$	Direction with the lowest particle count

Table 2 Table of symbols used in this section

As mentioned before, data from a single measurement can be used to estimate direction, although the distance d remains unknown. The simplest strategy would include moving in this direction as long as the particle count increases. This method could work for $h << d$, but as the UAV gets closer to the source, yaw stops being a dominant angle affecting the particle count. Hence, a slightly more complex solution was designed. The basic algorithm works as follows:

Algorithm 2 Solo localization

1: Set yaw = 0
2: **while** (yaw $< \pi$) **do**
3: Take k measurements $\rightarrow$ calculate sum
4: **if** (sum $<$ previous sum) **then**
5: Store $\vec{w_1}$ ▷ Forward direction of the UAV
6: **end if**
7: Increase yaw by θ
8: **end while**
9: Fly g meters in direction $\vec{w_1}$
10: **repeat** $1. - 8.$ to get $\vec{w_2}$
11: Rotate $\vec{w_1}$ and $\vec{w_2}$ by $\frac{\pi}{2}$
12: $S = \vec{w_1} \cap \vec{w_2}$
13: Fly towards S

A few additional steps have been added during tests in Gazebo:
Both of the two measurements can produce the same, or very similar direction. This leads to estimations, which lie far outside the area of operation. On the other hand, getting too close to the source can trigger the problem shown in Figure 13. This causes huge decrease in accuracy for $d < |g|$, as shown in Figure 16c. To solve both issues, the distance between UAV and the source (d) is calculated after every estimation. Three zones were created empirically, based on the distance:

- $d > 150$ - Estimation was probably incorrect. Go back to previous position and take more samples.
- $150 \geq d \geq 1.5g$ - Normal behaviour. Fly towards the estimated position, but only for 70% of the distance.
- $d < 1.5g$ - Getting very close to the source. Fly towards the estimated position, but only for 40% of the distance.

5.3 Formation of UAVs

This section explains the control algorithm for a formation of three UAVs to locate a single radiation source. This method implements a Kalman filter for sensoric data fusion and system state estimation. Basic Kalman filter is an optimal linear estimator, however, this system is strongly non-linear. For example, the relationship between UAV's yaw and measured particle count is a cosine-like function. For this reason, a non-linear variant, the Unscented Kalman filter (UKF) has been chosen.

The UAVs move in a fixed formation, where one UAV serves as a leader and the other two as followers. Shape of the formation and its influence on measurement accuracy is explained in Section 5.3.2.

In the beginning, the UAVs conduct a sweep scan of the entire area by flying in a sawtooth-like pattern shown in Figure 14. This results in a rough radiation heatmap, which is then used to set an initial state vector of the UKF. Position of the source, as estimated by the UKF, is then used as a target position for the center of the formation. The entire process results with the formation hovering steadily in one place with the radiation source being in the center. This approach is expected to be superior to the solo localization in both accuracy and speed, because multiple measurements can be done in different positions simultaneously.

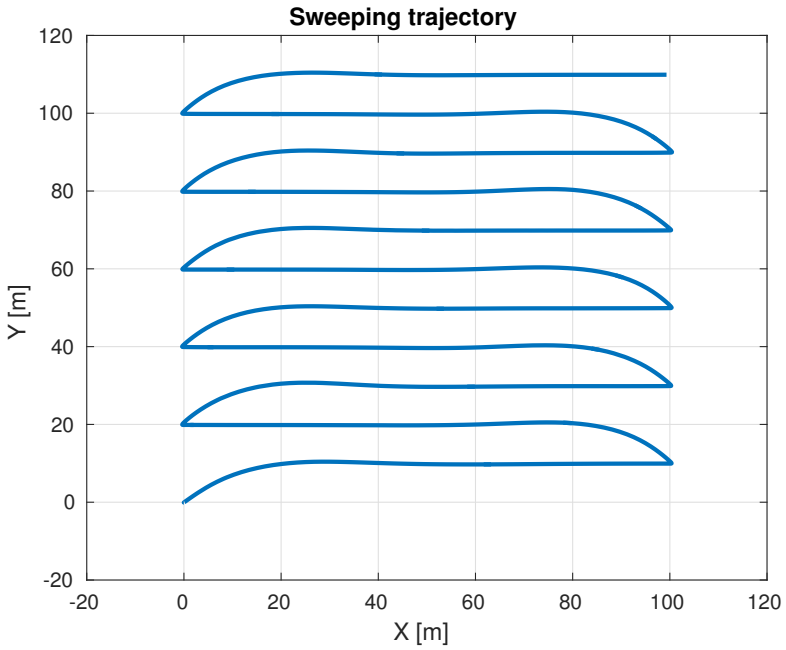

Figure 14 The formation conducts a fast sweep scan of the operational area by flying in a zig-zag pattern. Resulting data are then used to initialize an Unscented Kalman filter.

5.3.1 Unscented Kalman filter

The UKF is a non-linear state estimation algorithm, which provides an optimal solution, provided an accurate system model is used. A detailed description of the algorithm presented in [42] was used to implement the UKF in ROS. When compared to another non-linear variant, the Extended Kalman filter (EKF), the UKF yields slightly better results according to [43] and [42], especially when used with strongly non-linear systems.

The system can be described by a discrete, non-linear state space model, by using Equations 4, 5. All symbols used in this chapter are listed in Table 3.

$$\vec{\chi_k} = \vec{f}(\vec{\chi_{k-1}}, \vec{u_k}) + \vec{v_k} \tag{4}$$

$$\vec{z_k} = \vec{h}(\vec{\chi_k}) + \vec{w_k} \tag{5}$$

Symbol	Description
$\vec{\chi}$	System state estimation
$\vec{u}$	System input vector (sensoric data)
$\vec{z}$	System state observations
$\vec{v}$	Process noise
$\vec{w}$	Observation noise
$\vec{f}$	Non-linear function used to predict current system state
$\vec{h}$	Non-linear function mapping system states to the output
x_i	X coordinate of i-th UAV
y_i	Y coordinate of i-th UAV
s_x	X coordinate of the radiation source
s_y	Y coordinate of the radiation source
θ_i	Yaw of i-th UAV
φ_i	Ideal yaw[2] for i-th UAV
a_i	Radiation intensity in position of i-th UAV
a_{m_i}	Maximum possible intensity in position of i-th UAV

Table 3 Table of symbols used in this section. The noise is assumed to be Gaussian and non-additive.

The vectors used in this section are defined as

$$\vec{\chi} = (x_1, y_1, x_2, y_2, x_3, y_3, \theta_1, \varphi_1, \theta_2, \varphi_2, \theta_3, \varphi_3, s_x, s_y, a_{m_1}, a_{m_2}, a_{m_3})^T,$$
$$\vec{u} = (x_1, y_1, x_2, y_2, x_3, y_3, \theta_1, \theta_2, \theta_3, a_1, a_2, a_3)^T$$

[2] At this angle is the detector pointed directly towards the source

and the non-linear function $\vec{f}$ is defined as

$$\vec{f} = \begin{bmatrix} \mathbf{I}_{7\times 1} \\ atan2\left(\frac{s_y - y_1}{s_x - x_1}\right) \\ 1 \\ atan2\left(\frac{s_y - y_2}{s_x - x_2}\right) \\ 1 \\ atan2\left(\frac{s_y - y_3}{s_x - x_3}\right) \\ \frac{x_1a_1 + x_2a_2 + x_3a_3}{a_1 + a_2 + a_3} \\ \frac{y_1a_1 + y_2a_2 + y_3a_3}{a_1 + a_2 + a_3} \\ \frac{a_1}{cos(\theta_1 - \varphi_1)} \\ \frac{a_2}{cos(\theta_2 - \varphi_2)} \\ \frac{a_3}{cos(\theta_3 - \varphi_3)} \end{bmatrix}.$$

The states, which can be measured (position and yaw of the UAVs) are directly assigned the value from current measurement (ones in function $\vec{f}$), while the other states are calculated using current measurement and states from a previous step.

The output mapping function $\vec{h}$ is identity in this case. This means that the estimated states are directly used in the control loop.

The entire process is centralized, the estimation is done onboard the leader UAV and the followers only recieve new target coordinates. This is done in order to minimize necessary communication and avoid delays. The radiation intensity readout is done with a frequency of 1 Hz. Thus, the estimation is done with the frequency of 1 Hz as well.

5.3.2 Formation shape

In order to maximize the directional coverage, each UAV is rotated to a different yaw. For three UAVs and rotation interval $< 0; \pi)$ radians, the solution is to set the yaw with $\frac{\pi}{3}$ radians apart. The formation movement is triggered by a difference in measured radiation intensity. The entire formation is pulled in a direction of the strongest measurement. The estimation is the most accurate, when all three lines projected from the detectors intersect in one point. This is accomplished by placing the UAVs in the vertices of an equilateral triangle and having the detectors face towards the center. When all three UAVs detect the same radiation intensity, the source is located at the center of the triangle.

6 Simulation results

This section contains results of experiments performed in the simulator Gazebo. These experiments were conducted to demonstrate functionality of previously described algorithms and to find suitable parameters for use in the real system.

The goal of each experiment is to find an exact position of the radiation source. To evaluate the results, an estimation error is calculated as an Euclidean distance between the estimated position and the real position of the source. Another important factor is the time required to complete the task. In the simulations, the UAVs are not limited by a battery life. However, the purpose of these simulations is to prepare the system for use onboard real UAVs. Therefore, the time consumption was also considered during the tuning of system parameters.

6.1 Single UAV

The Algorithm 2 showed a major flaw during initial testing. As the UAV got close to the source, the localization accuracy significantly decreased. This can be seen in Figure 16. The cause was a combination of two issues, both of which have been explained in previous chapters - yaw stopped being a dominant angle, and the source appeared inside the detector model. This problem was eliminated by introducing the three zones of movement described in Section 5.2.

The experiments were all done with settings listed in Table 4. Only position of the source $\vec{S}$ and the rotation step θ were different for each experiment. The initial distance between the UAV and the source was never larger than 50 meters to ensure that some particles reach the detector.

Param.	Value	Meaning
h	5 m	Altitude of the UAV
g	15 m	Distance between measure points
k	5	Number of samples
(X, Y)	$(0, 0)$	Initial coordinates of the UAV
m	50 g	Mass of the ^{137}Cs (unless explicitly stated)

Table 4 Table of symbols used in this section

Figure 16 demonstrates the behaviour of the Algorithm 2 without any further additions. The localization accuracy is insufficient for any practical use, mainly because this approach is very likely to encounter the problem of a source appearing inside the detector model.

The first addition, aimed to remove this problem completely, is the introduction of three zones, which limit the UAV's movement based on the distance from the estimated source position. The limitation, preventing the UAV from getting too close to the source can be clearly seen in Figures 17a, 17b and the improved accuracy in Figure 17c.

To further increase the precision of the solo localization, the UAV needs to make smaller rotation steps. However, the more rotation steps are made, the more time is

required for every iteration. To reduce the time-consumption, while still retaining a high precision, the number of steps is changed progressively. Figure 18 demonstrates an approach using a high number of steps in the beginning, which is then reduced after every iteration. The main motivation for using a high number of steps in the beginning is to minimize the error during the first few iterations, when the UAV is expected to cross the largest distance. An opposite approach is shown in Figure 19, with a smaller number of steps in the beginning, which increases after every iteration. Of all the tested configurations, the increasing step count has yielded the best results with 8 rotation steps in the beginning, increased by 1 after every iteration, stopped at 16. A simulation with these parameters was launched 14 times, with the source being placed in varying randomly generated positions inside a circle with radius of 50 meters around the starting position. The performance was analyzed by calculating a mean average and variance of the simulation results. Each of the simulations required more than 30 minutes to finish 11 iterations. The time requirements are far too large for a real helicopter. Therefore, only 3 iterations will be done with a real system (approximately 8 minutes). The third iteration was chosen as a final one because of the best average results in the performance analysis, as shown in Figure 20. Snapshots from the simulations are shown in Figures 15, 21. Figure 15 shows the final position of the UAV after several iterations, while Figure 21 shows one of the experiments in progress. A full video from one of the simulations, which neatly demonstrates the whole solo localization process, is avaliable online at `https://www.youtube.com/watch?v=x8hacOAcJlY`.

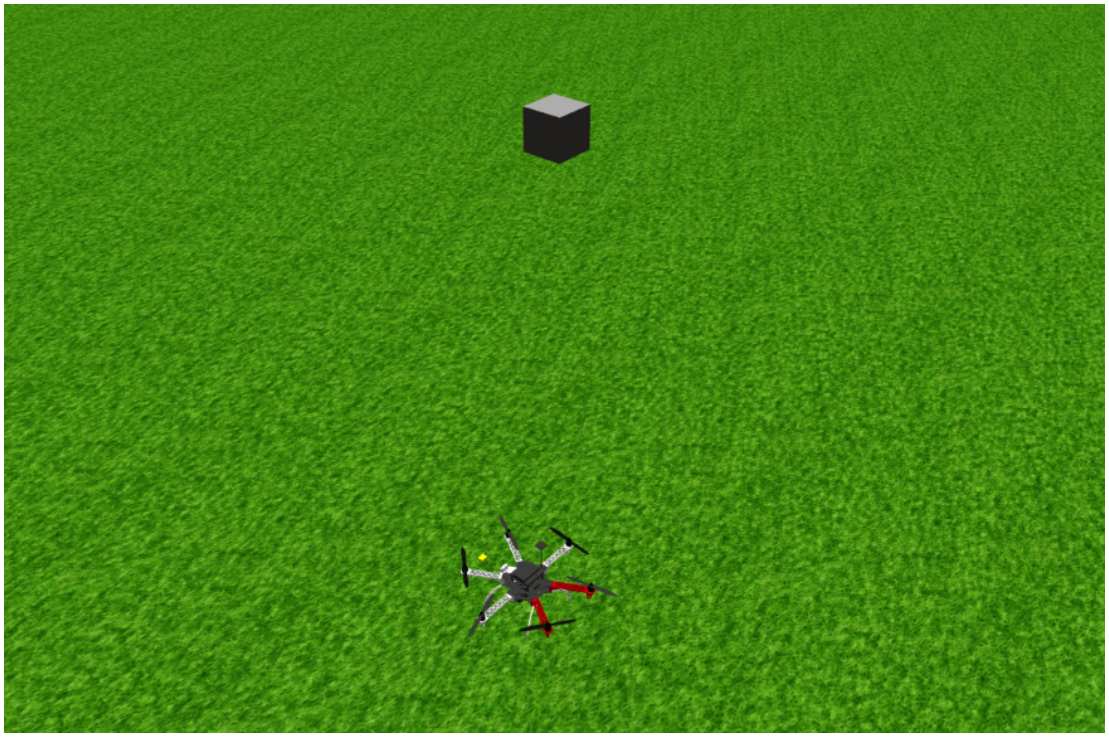

Figure 15 A snapshot from Gazebo showing the UAV and a model of radioactive Cesium-137 (represented by a grey box). The Timepix model is not visualised, however, the direction in which the model is currently facing is marked by a yellow dot next to the UAV.

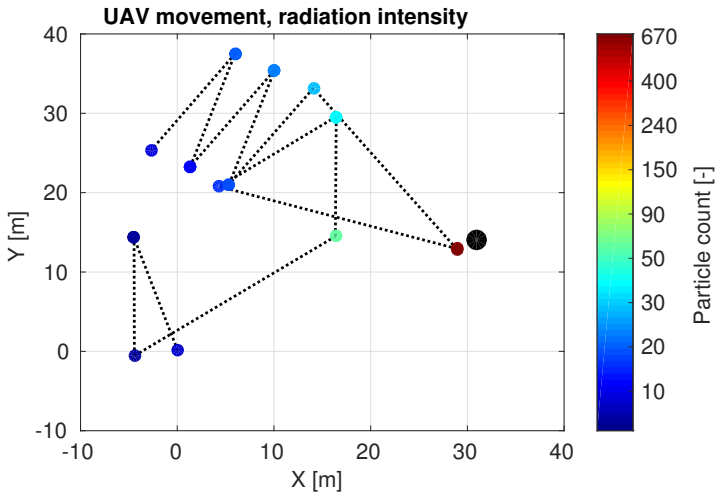

a) Movement of the UAV between measurement positions. The strongest radiation intensity measured in every point is highlighted by a coloured circle.

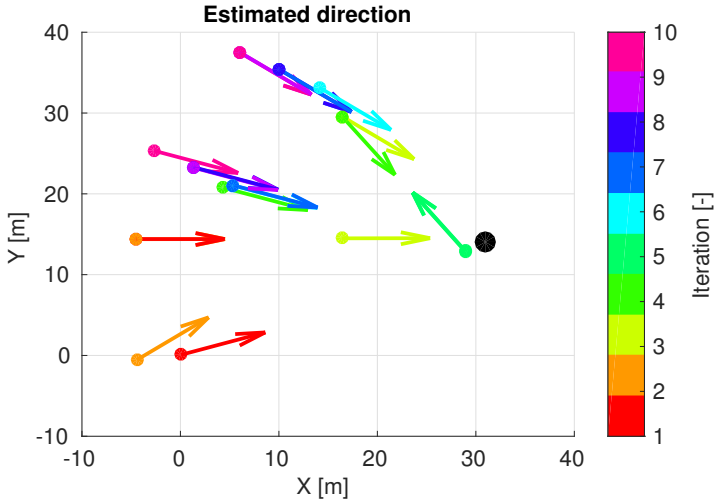

b) Arrows denote an estimated direction towards the source. Notice the arrow pointing away from the source during iteration 5. This is a result of the model imperfection explained Section 5.1.

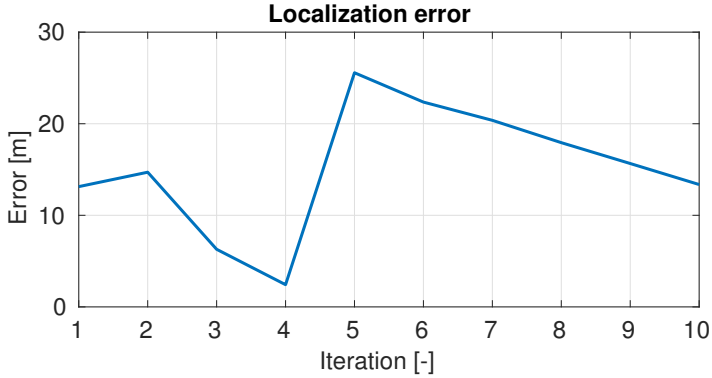

c) Euclidean distance between an estimated position and the real position of the source.

Figure 16 Localization with the bare Algorithm 2. The radiation source is placed in position $(31, 14)$ (marked by a black dot). The number of rotation steps n was set to 10. The lacking accuracy of this approach was improved by adjustments described in Section 5.2.

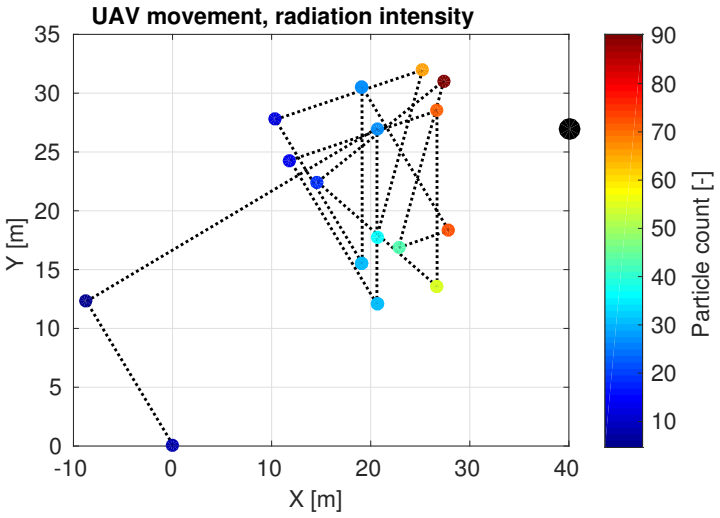

a) Movement of the UAV between measurement positions. The strongest radiation intensity measured in every point is highlighted by a coloured circle.

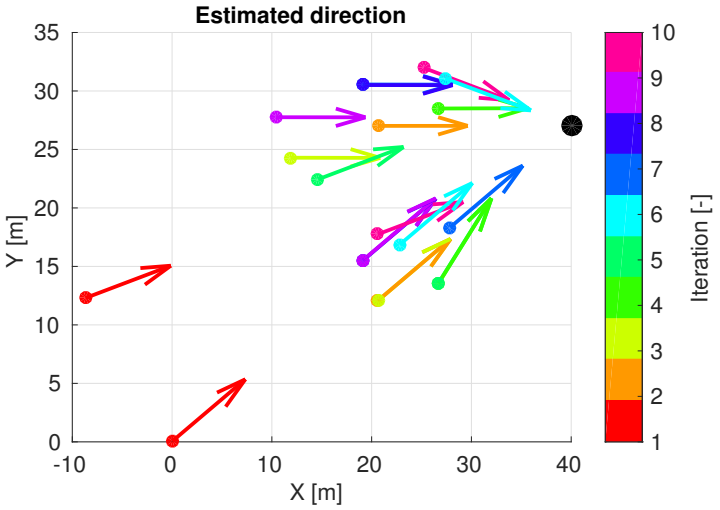

b) Arrows denote an estimated direction towards the source. To calculate an intersection of two lines, two measurement points are needed. Two points used in the same iteration are highlighted with the same colour.

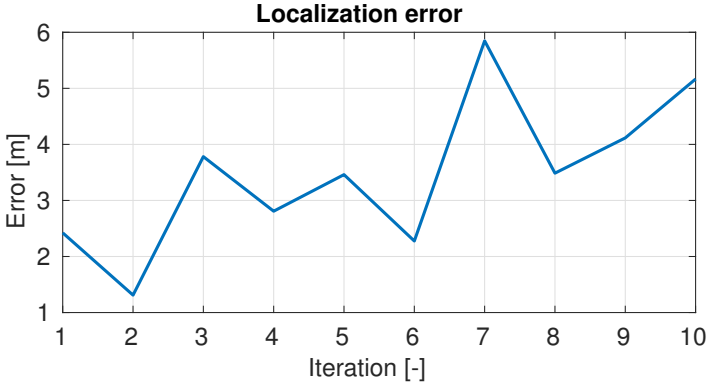

c) Euclidean distance between an estimated position and the real position of the source.

Figure 17 Algorithm 2 after the addition of the three zones mentioned in the Section 5.2. Radiation source is placed in position $(40, 27)$ (marked by a black dot). The number of rotation steps n is set to 8. This figure demonstrates the improvement caused by the introduction of the zones.

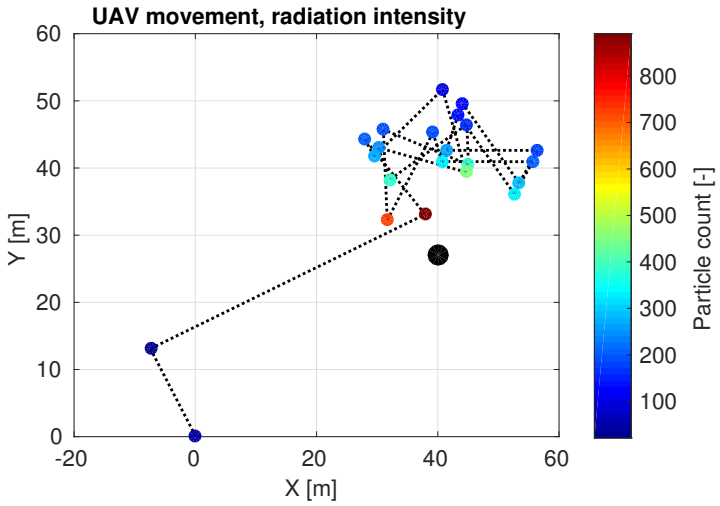

a) Movement of the UAV between measurement positions. The strongest radiation intensity measured in every point is highlighted by a coloured circle.

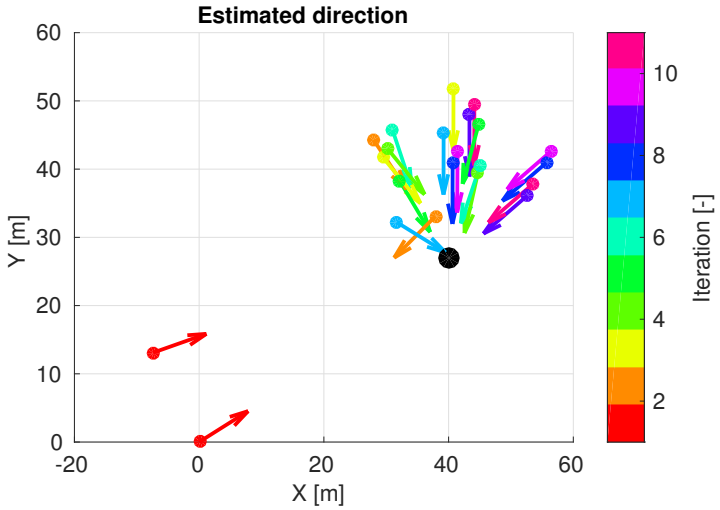

b) Arrows denote an estimated direction towards the source. Notice the arrow pointing away from the source during the second iteration. This is caused by an imperfection of the detector model explained in Section 5.1.

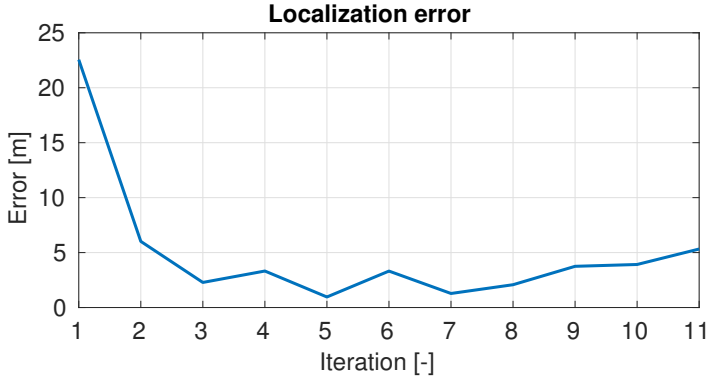

c) Euclidean distance between an estimated position and the real position of the source.

Figure 18 Another addition to improve precision is to change the number of rotation steps. Radiation source is placed in position $(40, 27)$ (marked by a black dot). The number of rotation steps n is set to 16 and decreased by 1 after every iteration (stopped at 8).

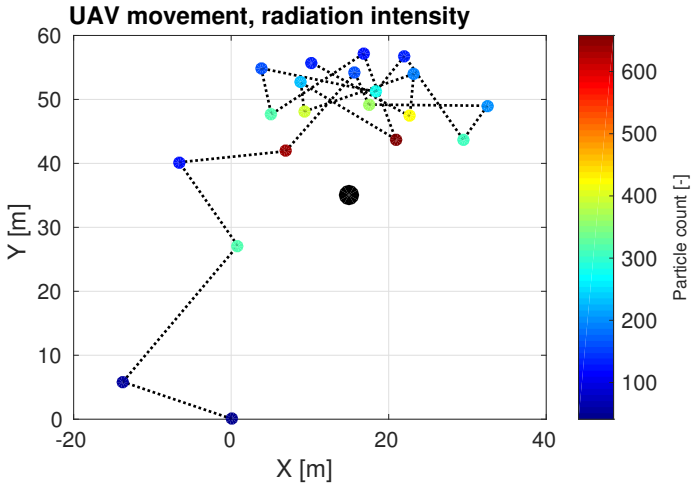

a) Movement of the UAV between measurement positions. The strongest radiation intensity measured in every point is highlighted by a coloured circle.

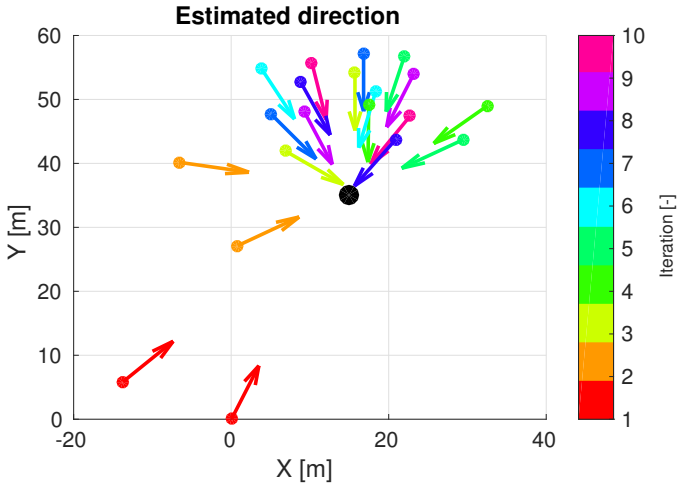

b) Arrows denote an estimated direction towards the source. To calculate an intersection of two lines, two measurement points are needed. Two points used in the same iteration are highlighted with the same colour.

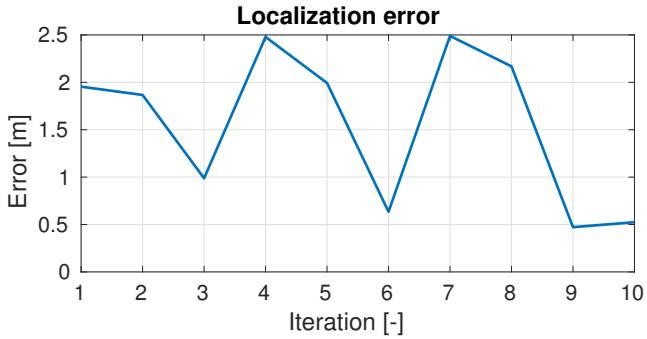

c) Euclidean distance between an estimated position and the real position of the source.

Figure 19 Radiation source is placed in position $(15, 35)$ marked by a black dot. The number of rotation steps n is set to 8 in the beginning and increased by 1 after every iteration (stops at 16). When compared to all previous measurements, this approach yields by far the best results.

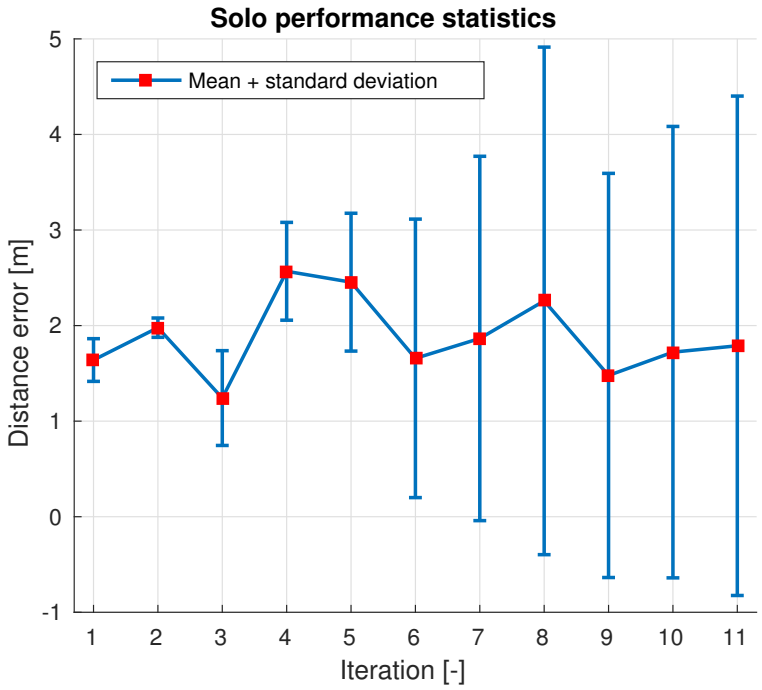

Figure 20 Statistical analysis of the solo performance. The simulation was launched 14 times with the same parameters as in previous experiment: number of rotation steps set to 8, increasing by 1 after every measurement (capped at 16). The position of the source was selected randomly for each simulation. Average estimation error (red) and standard deviation (vertical bars) are shown in the graph.

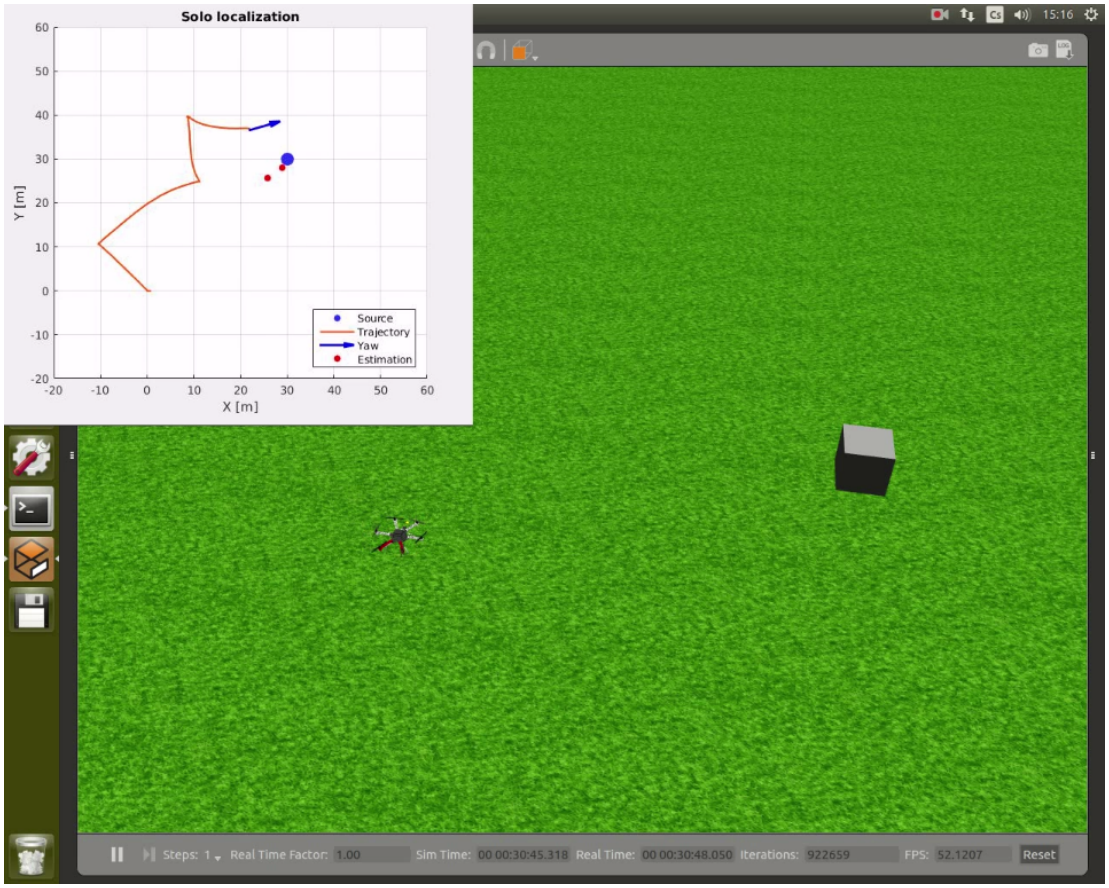

Figure 21 Another snapshot from Gazebo showing a complete trajectory, which the UAV has created until this point during an experiment. This snapshot was taken during the performance analysis (see Figure 20) and the UAV uses the improved variant of the solo algorithm. A complete video of this simulated experiment is avaliable online at `https://www.youtube.com/watch?v=x8hacOAcJlY`.

6.2 Formation of UAVs

Initial sweeping provides a coverage of the entire operational area. Therefore, the UAVs do not need to detect any particles from the initial position. This allows detection of a very weak source (e.g. 10 gramms of ^{137}Cs) in a very large area, theoretically limited only by a battery life of the UAVs.

The result of this sweeping is a 2D array of points scattered over the area of operation. The empty spaces between those points are filled by using a linear interpolation, which results in a rough map of radiation intensity. The area with the highest particle count is then used as an initial state for the UKF. This approach resulted with an estimation error of less than 2 meters for all formation sizes from 5 to 40 meters. However, some formations struggle, when attempting to recover from a bad initialization. The relationship between formation size and recovery speed was found experimentally. The UKF was initialized with a distance error equal to 50% of the formation size and the time required to reduce this error steadily under 1 meter was measured. The simulation was launched 10 times for all formation sizes a, where $a = \{5, 6, ..., 25\}$ m. Analysis of the simulation results is presented in Figure 22. These results show, that formation sizes from 15 to 21 meters provide the most reliable error suppression. Since all three UAVs will move in the same altitude, formation sizes under 10 meters were not considered for

safety reasons. A size of 15 meters was chosen for all further experiments.

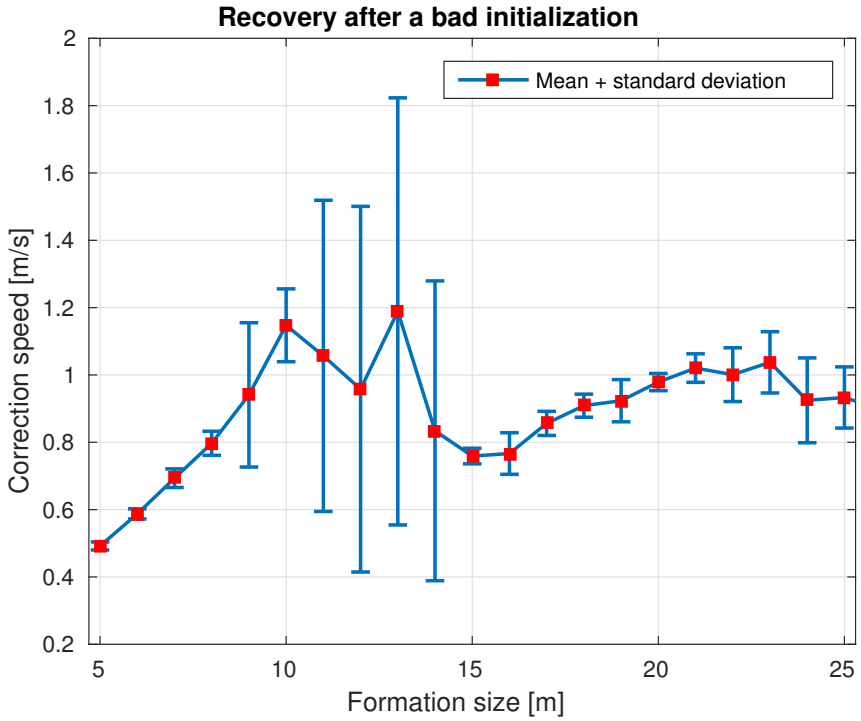

Figure 22 Statistical analysis of the formation performance. The UAVs are positioned in vertices of an equilateral triangle. The estimation algorithm is initialized with an error equal to 50% of the formation's size, and the time required for correction of the error is measured. The timer is stopped after the error remains under 1 meter for 10 consecutive seconds. This graph demonstrates, how fast different formation sizes recover from an incorrect initialization. The simulation was launched 10 times for each size. Mean average of the results (red marks) and the standard deviation (vertical bars) are presented in the graph.

Multiple simulations were launched to test the ability to localize the radiation source in various sections of the operational area. For all simulations, the formation is initially centered at coordinates $(0, 0)$ and the distance between UAVs is 15 meters. Variable parameters used in these simulations are listed in Table 5.

Param.	Meaning
x_d	Sweeping step in the direction of X axis
y_d	Sweeping step in the direction of Y axis
$\vec{s}$	Position of the radiation source
m	Mass of the ^{137}Cs

Table 5 Table of variables used in simulations of the cooperative searching.

Numerous different scenarios were tested in the simulator. Results of two of these experiments are presented in this section and they represent the best and the worst case scenario. The first experiment demonstrates the ability to find the source of radiation in a very large area. The source is placed near the center of this area and at least one of the UAVs will directly cross this position, which makes this a best case scenario. The simulation was launched with following parameters: $m = 50$ g, $x_d = 100$ m, $y_d = 20$ m, $\vec{s} = (36, 72)$. A snapshot taken during this experiment in Gazebo is shown in Figure

23. This figure shows the final position of the formation after a successful localization along with the evolution of an estimation error. For a full video of this experiment, visit `https://www.youtube.com/watch?v=6GEYo5El-zQ`. The data recieved from the initial sweeping is presented in Figure 24 and the evolution of localization error is shown in Figure 25.

Another experiment was conducted to test the ability to find the source in a corner of the area, which the sweeping formation nearly misses. This represents the worst case scenario, since the source will never occur in between the UAVs during the initial sweeping. The simulation was launched with following parameters: $m = 50$ g, $x_d = 35$ m, $y_d = 10$ m, $\vec{s} = (32, 5)$. Figure 26 shows the results on the initial sweeping and Figure 27 shows the corrections done during the precise localization.

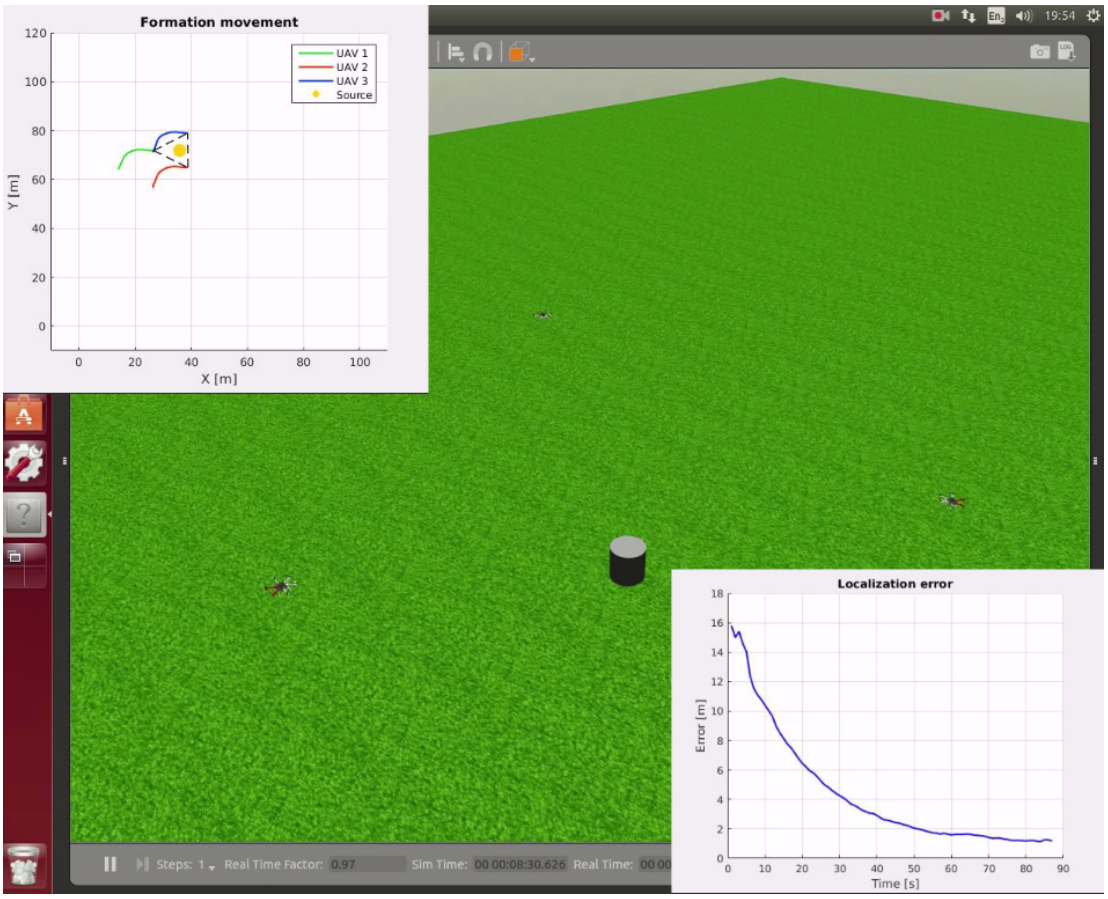

Figure 23 A snapshot from Gazebo showing the error correction done by the Unscented Kalman filter. After minor position adjustments, the UAVs form an equilateral triangle with the radiation source located at its center. A full video of this experiment is avaliable online at `https://www.youtube.com/watch?v=6GEYo5El-zQ`.

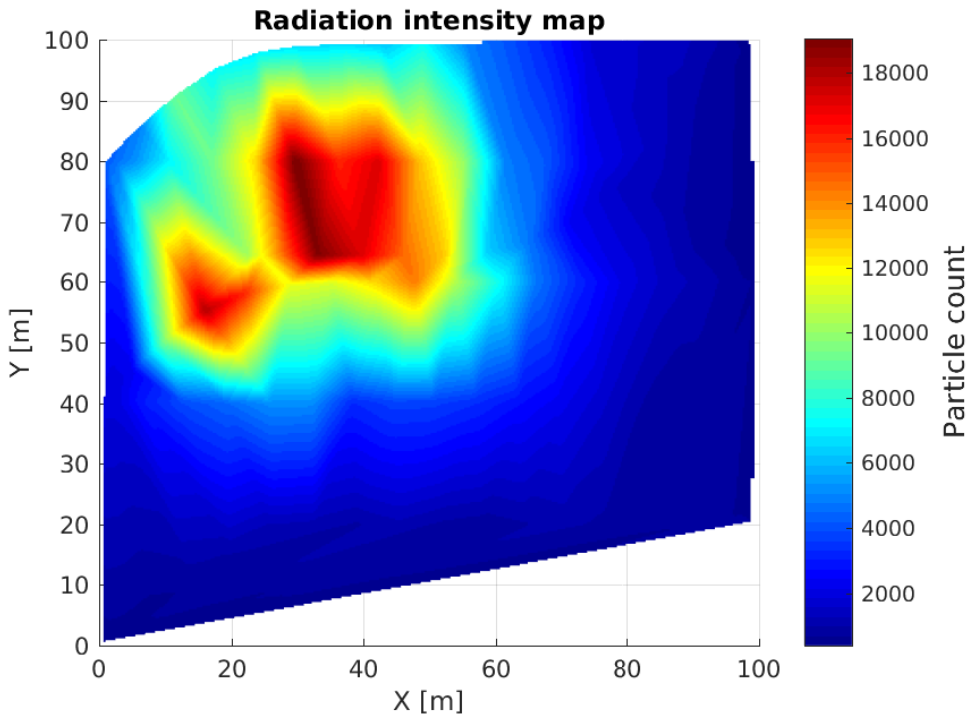

a) Radiation intensity map created using a linear interpolation of the measurements obtained during the initial sweeping of the area.

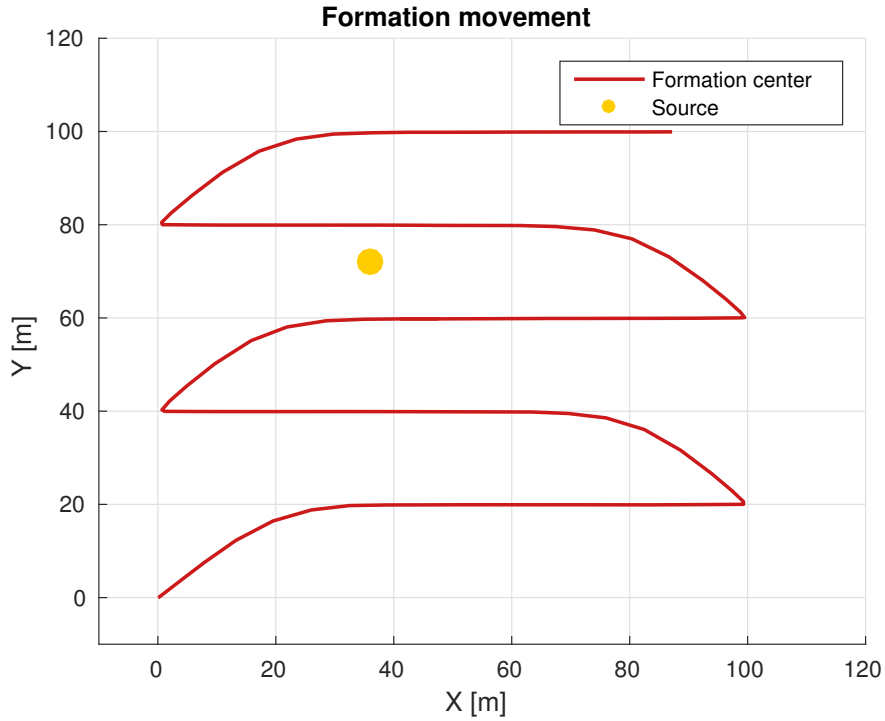

b) Trajectory which the formation has travelled during the initial sweeping. The radiation source is marked by a yellow dot.

Figure 24 Results of an experiment demonstrating the capability of locating a weak source of radiation in a large perimeter. The simulated source is placed at coordinates $(36, 72)$ and the activity is equal to 50 gramms of ^{137}Cs . A snapshot taken during this experiment in Gazebo is shown in Figure 23.

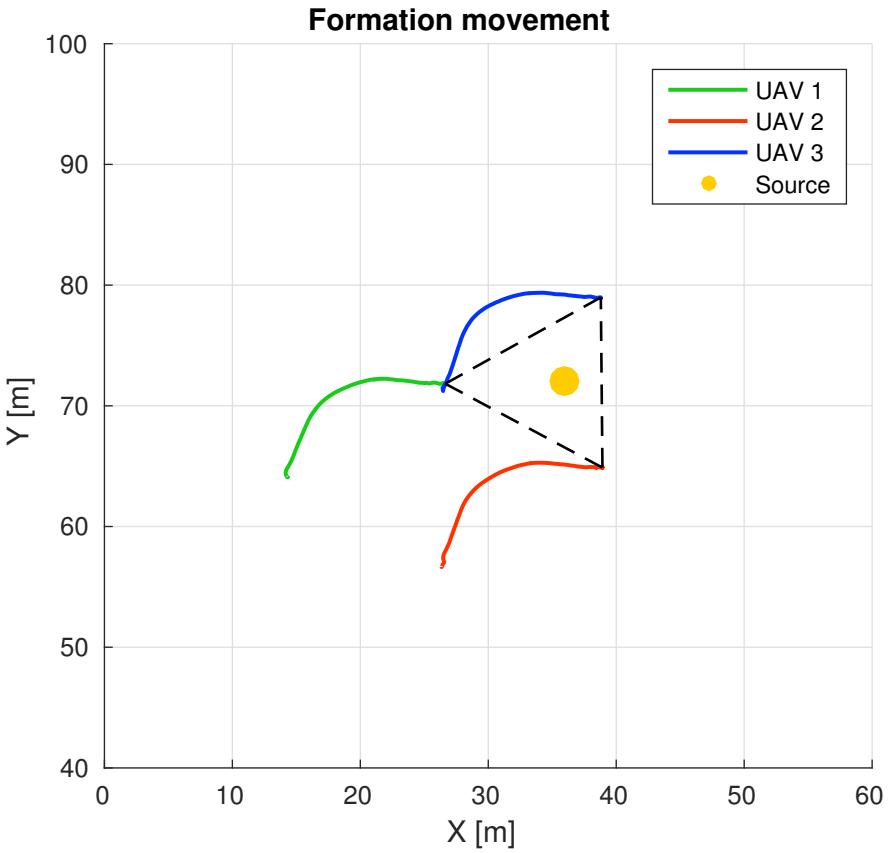

a) Movement of the formation during the precise localization and, caused by corrections of the estimated source position by the Unscented Kalman filter.

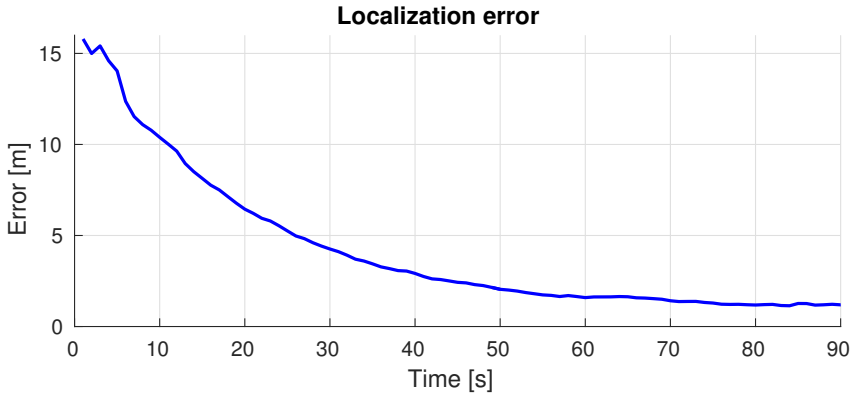

b) Evolution of the estimation error over time.

Figure 25 After the sweeping shown in Figure 24, the formation moves to the area with the highest measured intensity and a precise localization begins. The position of each UAV is slightly updated each second until the optimal solution is found. The optimal shape of the formation is an equilateral triangle with the source in its center, with all UAVs facing towards the center with the detectors. For a full video of this experiment visit `https://www.youtube.com/watch?v=6GEYo5El-zQ`.

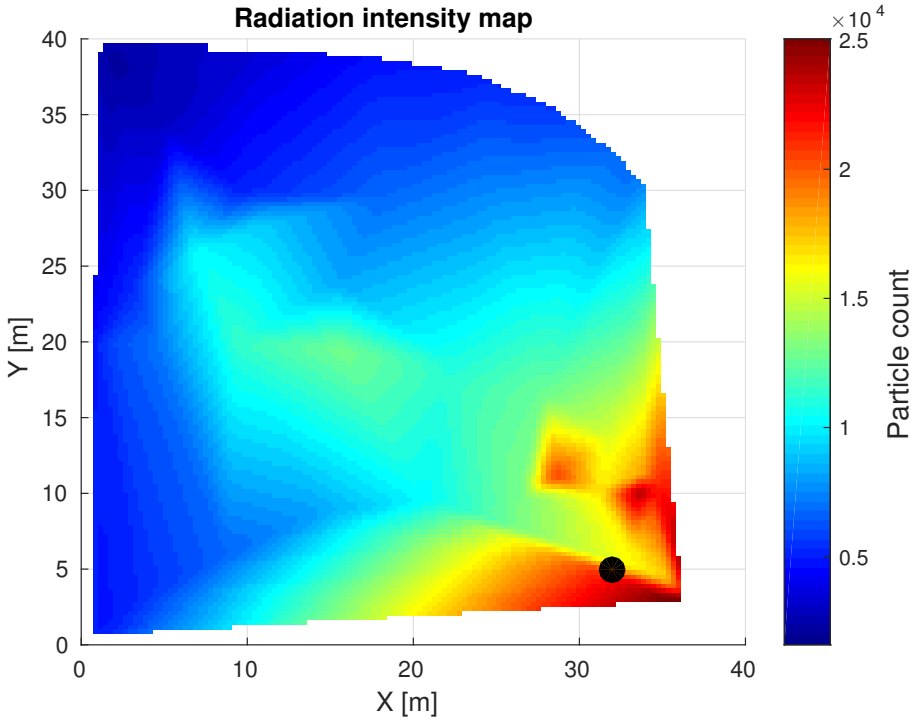

a) Radiation intensity map created using a linear interpolation of the measurements obtained during the initial sweeping of the area. The radiaton source is marked by a black dot.

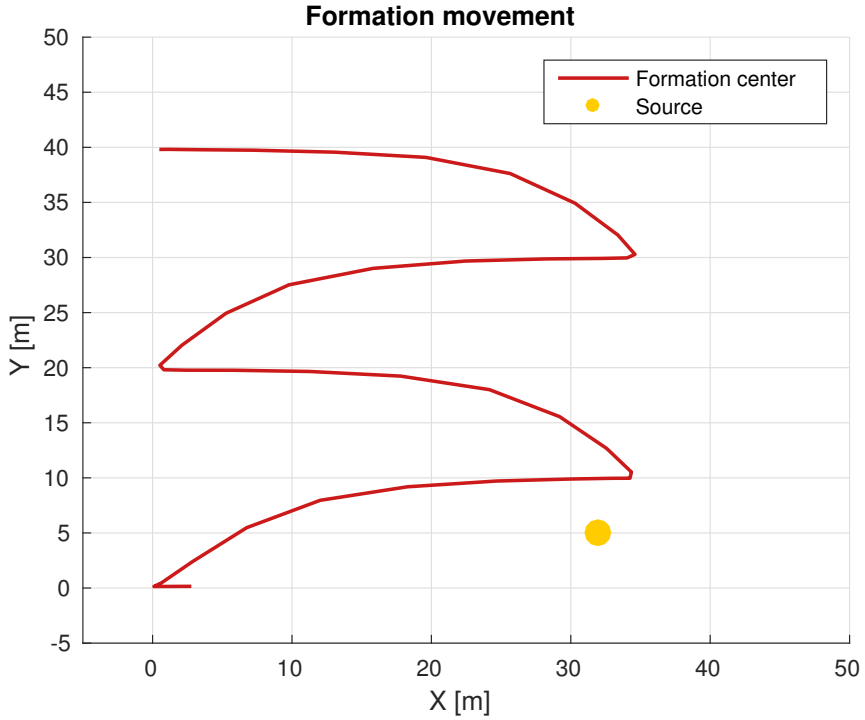

b) Trajectory which the formation has travelled during the initial sweeping. The radiation source is marked by a yellow dot.

Figure 26 Results of an experiment demonstrating the capability of locating a source of radiation in a corner of the area, which the formation nearly misses.

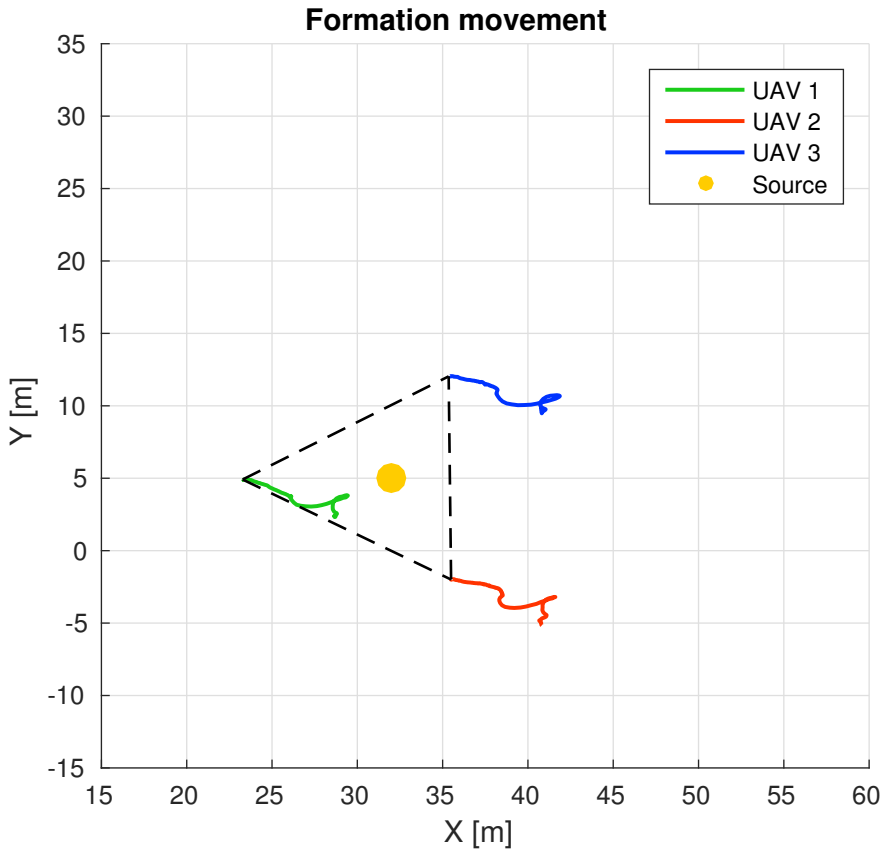

a) Movement of the formation during the precise localization and, caused by corrections of the estimated source position by the Unscented Kalman filter.

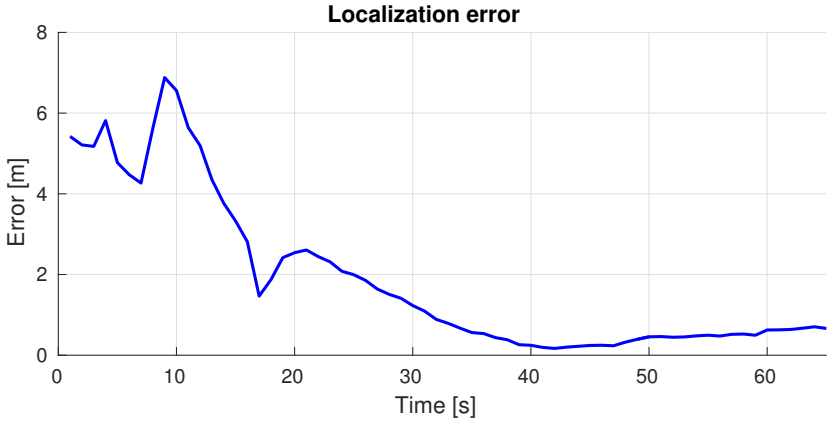

b) Evolution of the estimation error over time.

Figure 27 After the sweeping shown in Figure 26, the formation moves to the area with the highest measured intensity and a precise localization begins. The position of each UAV is slightly updated each second until the optimal solution is found. The optimal shape of the formation is an equilateral triangle with the source in its center, with all UAVs facing towards the center with the detectors.

7 Real experiments

This chapter presents results of experiments done with real UAVs. Unfortunately, a real radiation source was not avaliable because of strict safety regulations and the lack of closed areas, where the UAVs could fly freely. Nevertheless, the source can get replaced by the same simulated model as was used in the previous chapters. To avoid jamming the wireless communication, every UAV simulated an identical source at a frequency of 1 MHz using an onboard computer, while transmitting only the intensity measured by a simulated detector, at a frequency of 1 Hz. Both solo and cooperative approaches have been tested. Parameters for the real system were based on the most successful simulations.

The UAVs used in this project are built on a six-rotor platform DJI F550. They are equipped with multiple sensors, which enhance stability of the UAV and provide information about the surroundings. The algorithms rely on a relative localization of the UAVs, which was in these experiments provided by an RTK[1] module. The RTK uses signals from multiple satellite navigation systems to measure the exact coordinates of the UAV. Under ideal conditions, the measurement error is only a few centimeters. The UAVs are also equipped with a powerful onboard computer Intel NUC and use WiFi for communication.

The solo localization, shown in Figure 29, was done using parameters listed in Table 6. This experiment is very time-demanding, as the first iteration takes almost two minutes and every following iteration is even longer. With respect to battery limitations, the experiment was stopped after three iterations. This ammout of iterations also provided the most consistent results in the statistical analysis shown previously in Figure 20. Photos of a UAV performing the solo localization are shown in Figures 30a, 30b, 28.

Param.	Value	Meaning
h	5 m	Altitude of the UAV
g	15 m	Distance between measure points
k	5	Number of samples
m	50 g	Mass of the ^{137}Cs
(X, Y)	$(0, 0)$	Initial coordinates of the UAV
(S_X, S_Y)	$(-23, 25)$	Position of the radiation source

Table 6 Parameters used in a real experiment with one UAV.

The cooperative localization was tested two times with parameters listed in Table 7. The simulation was launched two times with the same parameters. Figures 31a and 33a show the radiation intensity map created after the initial sweeping. The map contains a lot more noise than the maps created during simulations in Gazebo. This is caused by an unsynchronized clock of the detector models. The leading UAV had to wait for particle count measurements from the two followers, which created gaps in the plot. This issue was left unsolved, because the localization algorithm successfully recovered after the noisy initialization. Evolution of the estimation error is shown in Figures 31b

[1] Real-time kinematics

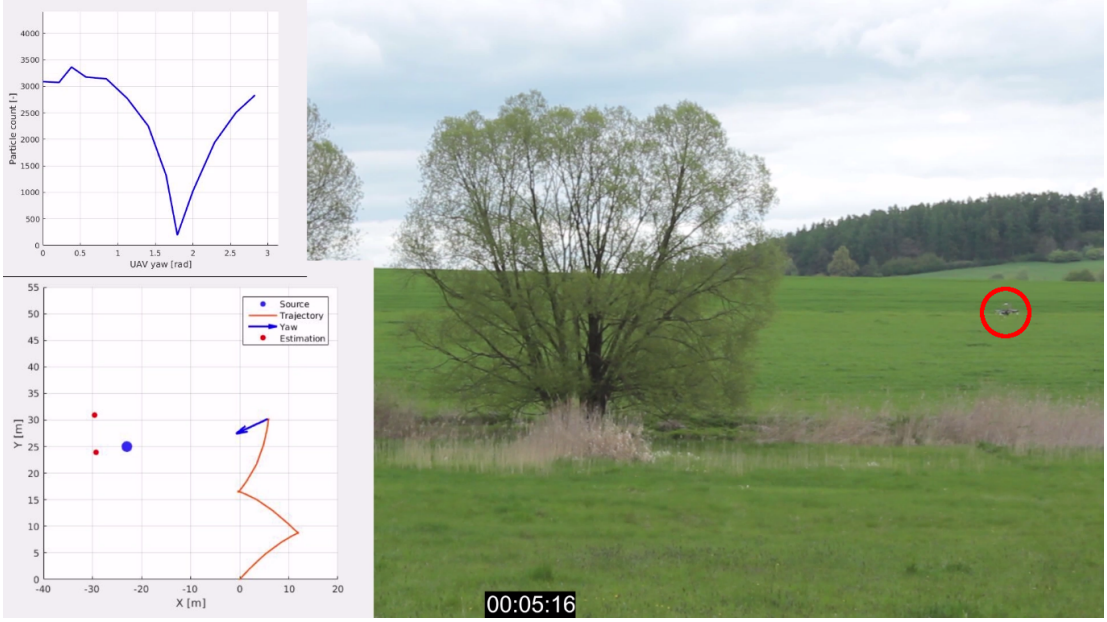

Figure 28 A snapshot from a video of a solo experiment, which is extended with graphs based on measured data. A full video of this experiment with animated measurement progress is avaliable online at `https://www.youtube.com/watch?v=_KBGdi1a2do`.

and 33b. In both cases is the estimation error stabilized under 1.6 meter after a few seconds. Figure 34 demonstrates the trajectory, which the formation followed during the initial sweeping. This trajectory remained the same for both experiments. Photos of the formation performing the cooperative localization are shown in Figures 35a, 35b, 35c and snapshots from a video are shown in Figures 36a, 36b. The full video with animated measurement progress can be viewed online at `https://www.youtube.com/watch?v=aZLEAHczIBw`.

Param.	Value	Meaning
a	15 m	Formation size, distance between UAVs
x_d	35 m	Sweeping step in the direction of X axis
y_d	10 m	Sweeping step in the direction of Y axis
(X, Y)	$(0, 0)$	Initial coordinates of the UAV
(S_X, S_Y)	$(31.5, 7.65)$	Position of the radiation source

Table 7 Parameters used in real experiments with a formation of UAVs.

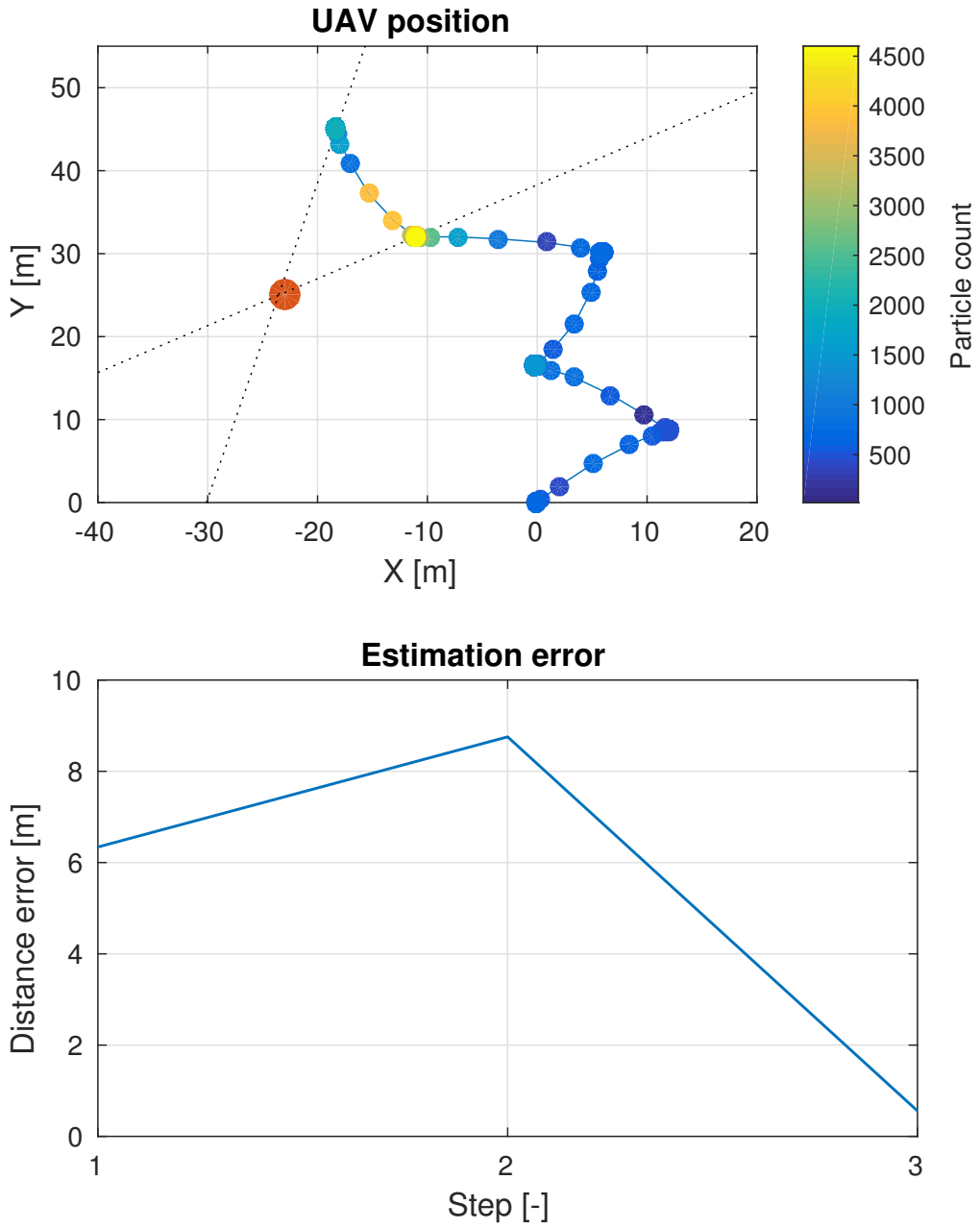

Figure 29 Results of a real experiment with one UAV. The upper graph shows the flight path and measured particle count. Two last direction estimates are marked with dotted lines and the actual position of the radioactive source is represented by an orange circle. The lower graph shows an evolution of estimation accuracy after each iteration.

a)

b)

Figure 30 Snapshots taken during the real experiment with one UAV. These photos show the UAV near the radiation source. The source was fully simulated, the white barrel only marks it's respective coordinates.

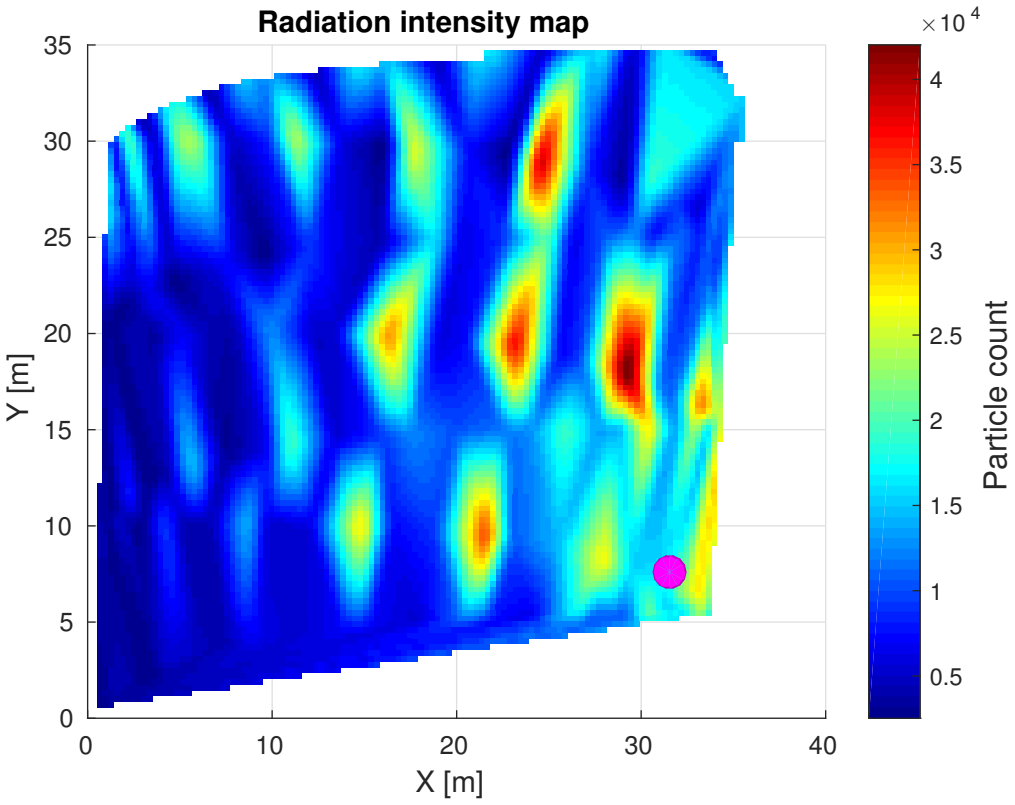

a) Map of radiation intensity obtained during the initial sweeping. An actual position of the radiation source is marked by a purple circle. The control system onboard the UAVs had no information about the source in the beginning of the experiment.

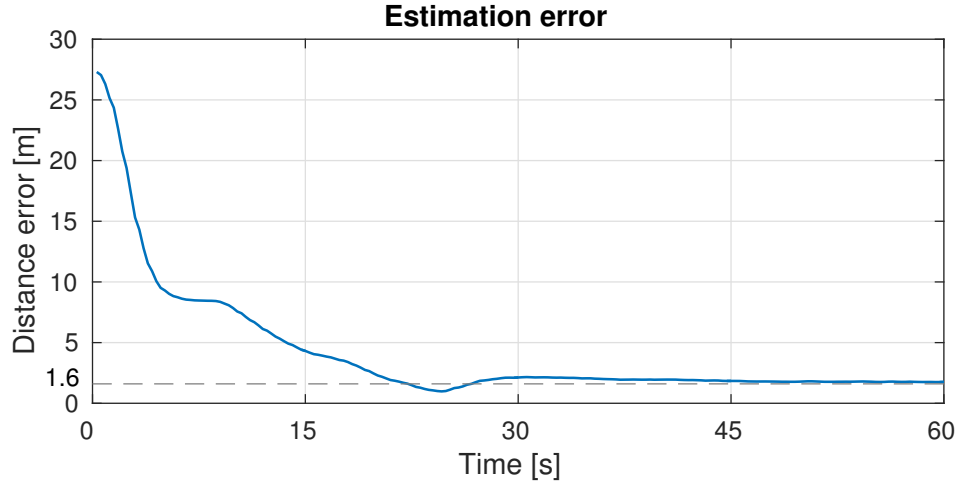

b) Evolution of an estimation error over time. Although the initial error is much larger than during simulations, a correction is performed very quickly. The estimation is stabilized with an error of 1.6 meters.

Figure 31 Processed data from the first run of the cooperative experiment with a real system. The measurement contains more noise than the data measured in simulator. The gaps in intensity map are caused by an unsychronized logging frequency of the three detector models. The leading UAV had to wait for measurements from the two followers during each cycle (once per second). The gaps also resulted with an incorrect initialization of the Unscented Kalman filter. The system, however, managed to find a correction and navigate the UAVs into the correct position.

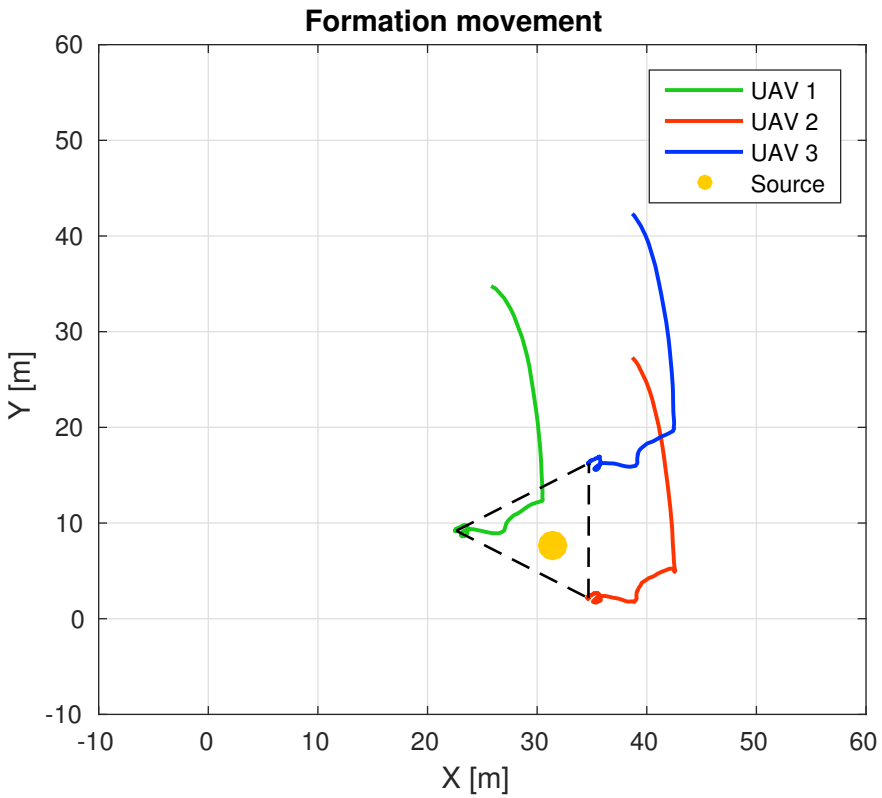

Figure 32 Movement of the formation during the correction of system parameters estimated by the Unscented Kalman filter. The accuracy of the localization is also affected by the quality of the relative localization, which was recieved from a satellite navigation system during this experiment.

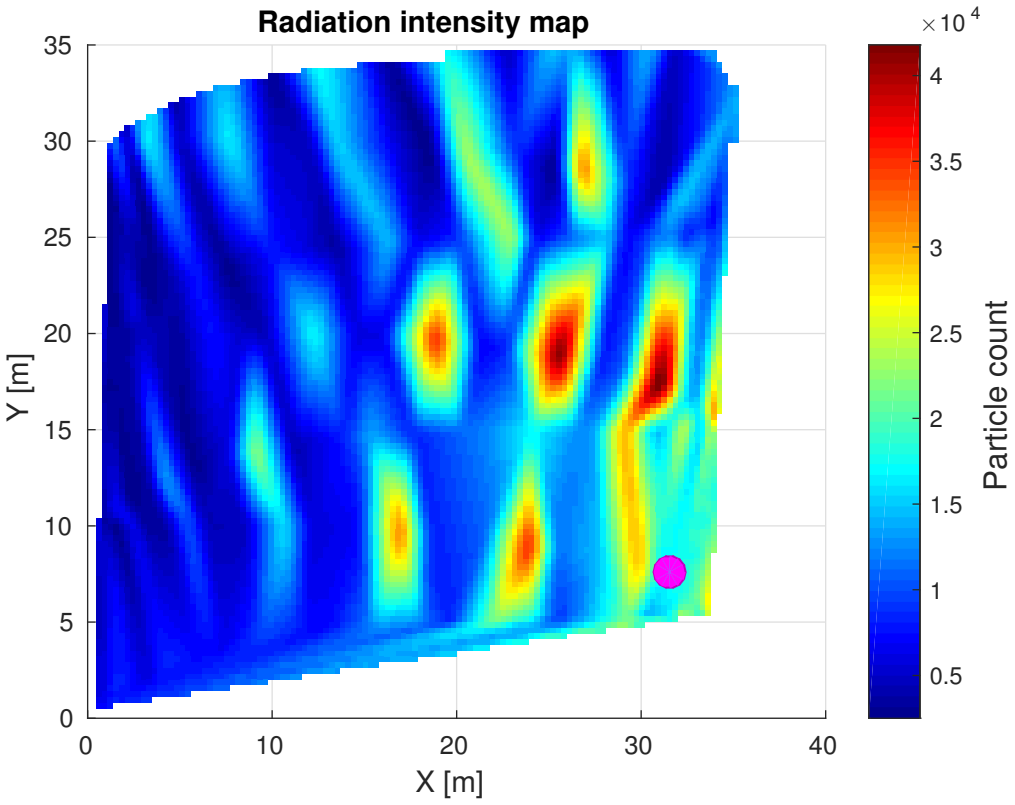

a) Map of radiation intensity obtained during a second run of the experiment with the same parameters. An actual position of the radiation source is marked by a purple circle. The control system onboard the UAVs had no information about the source in the beginning of the experiment.

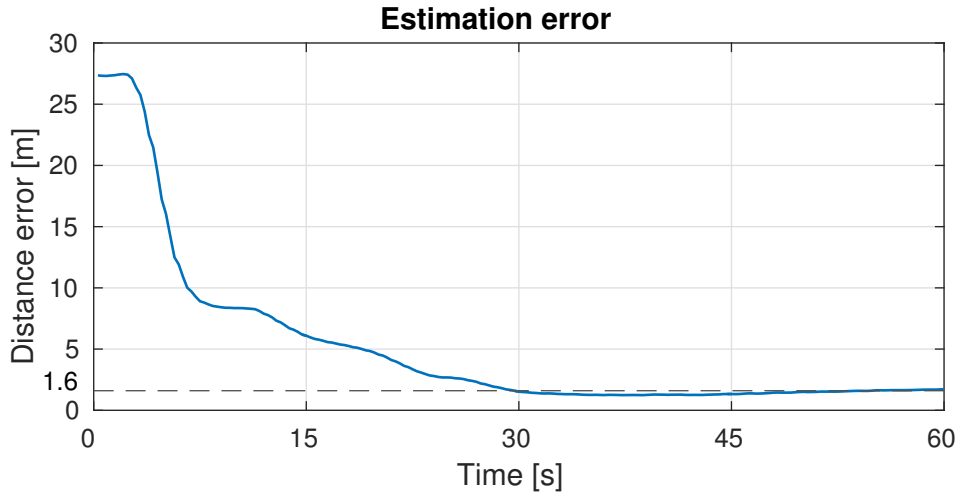

b) Evolution of an estimation error over time. The correction is slightly slower than during the previous run because of an even more inaccurate map. Nevertheless, the error correction is also stabilized around 1.6 meters.

Figure 33 Processed data from the second run of the cooperative experiment with a real system. This time, the initial sweeping provided an even more noisy map than in the previous case (Figure 31), which led to a slower, yet still successful correction of the estimated system parameters.

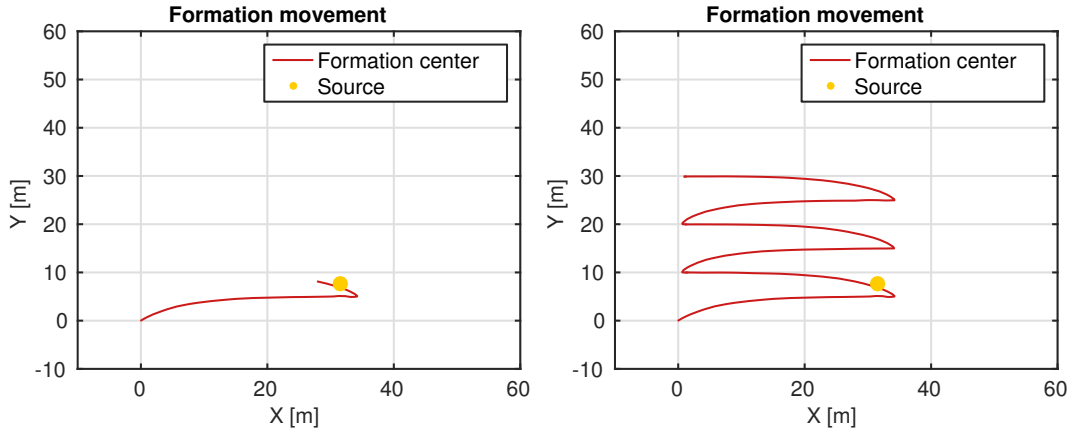

Figure 34 Sweeping trajectory used during the real experiments.

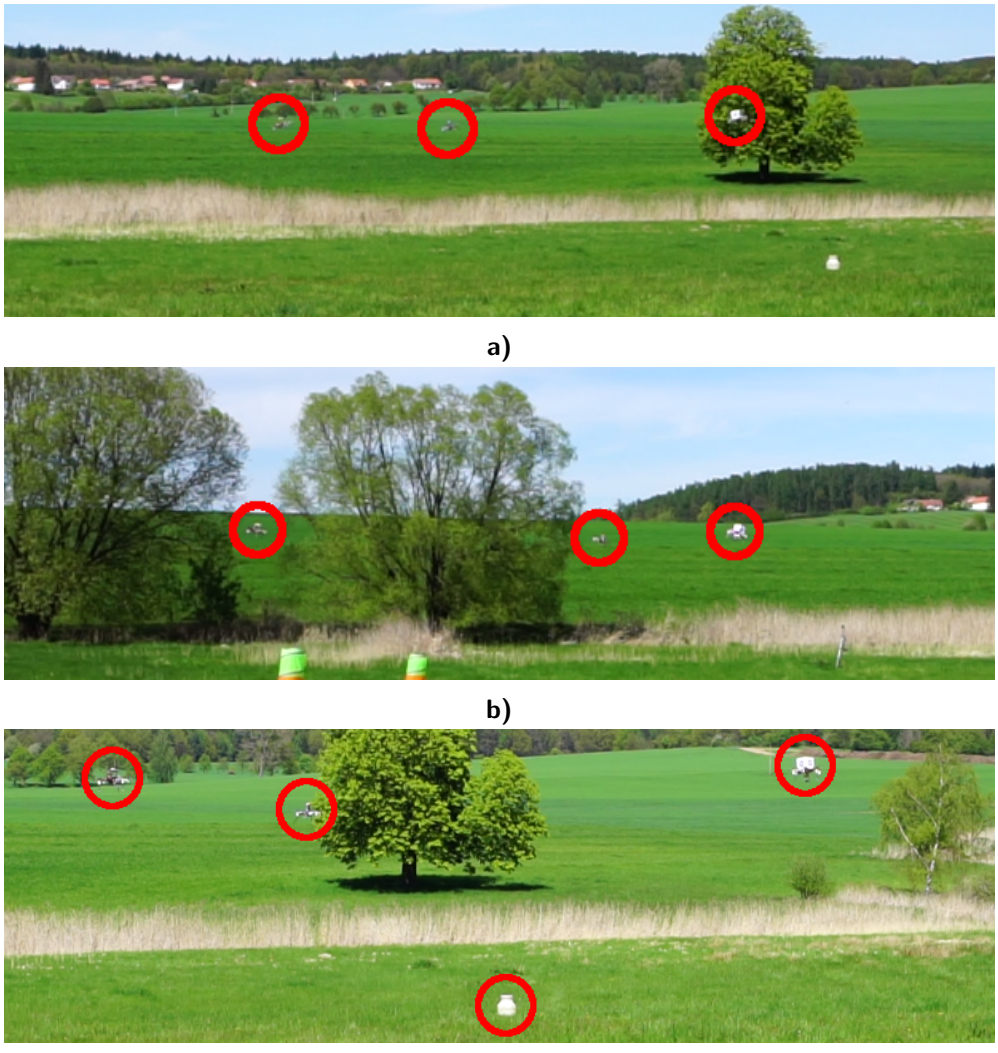

Figure 35 Snapshots of the formation during the real experiment. The first two images show the formation during the initial sweeping phase, in the third image the formation hovers in the final position above the radiation source (white barrel).

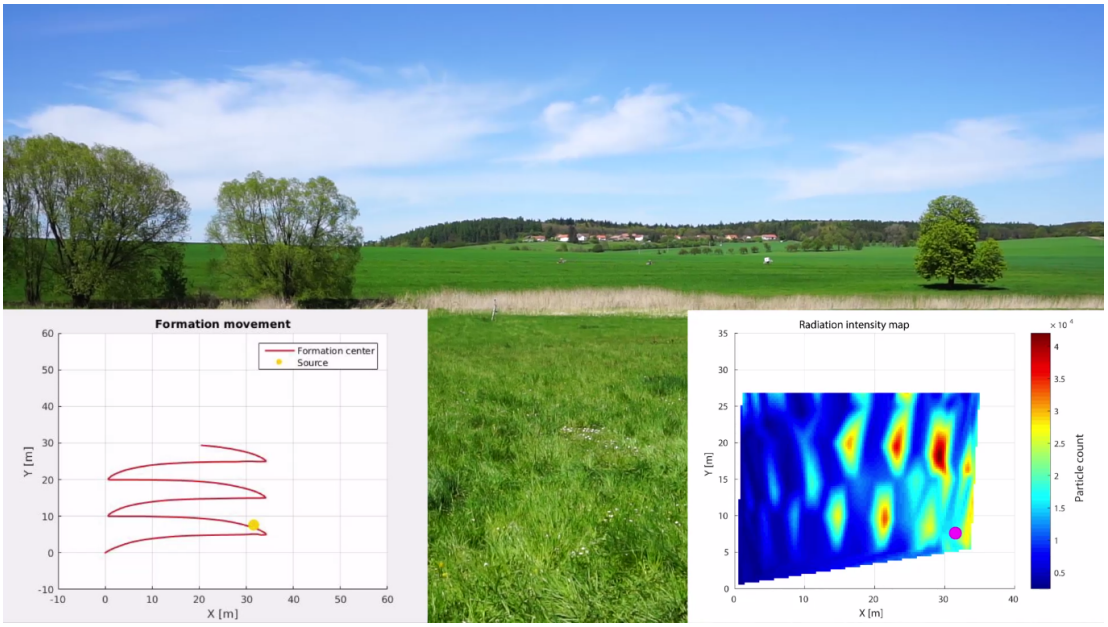

a)

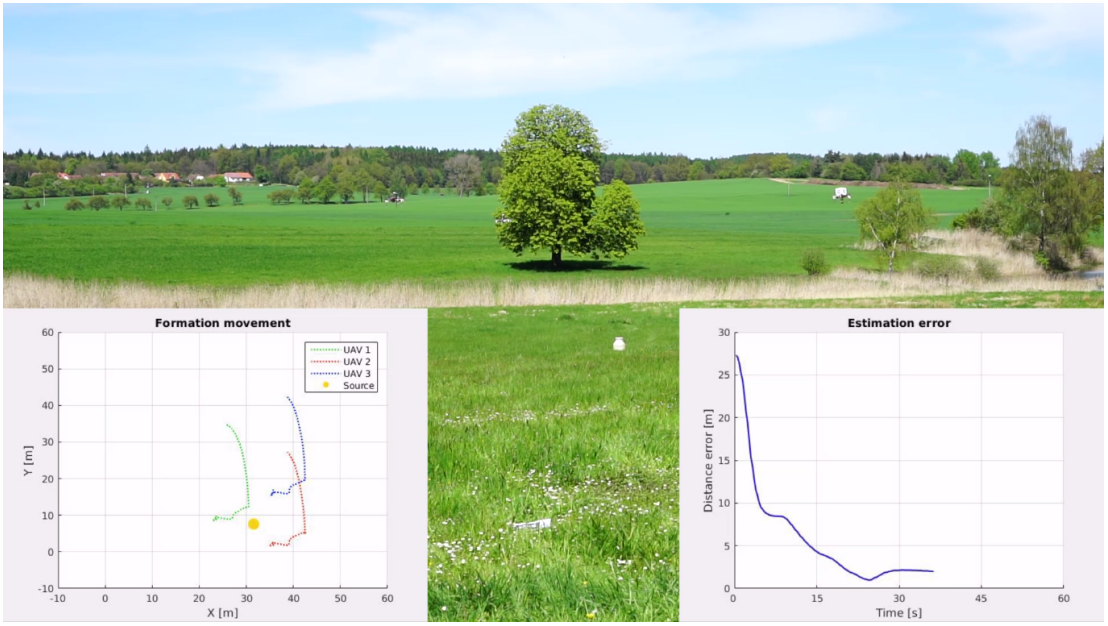

b)

Figure 36 Snapshots from a video demonstrating a full cooperative experiment extended with animated progress of the radiation measurements. The full video is avaliable online at `https://www.youtube.com/watch?v=aZLEAHczIBw`.

8 Conclusion

This thesis dealt with localization of a radiation source using unmanned aerial vehicles (UAVs). Because of problems linked with handling of radioactive materials, creation of a simulated radioactive enviroment was necessary. Models of a radioactive isotope, Cesium-137, and a particle detector Timepix were designed and implemented in the robotic framework ROS and experimentally verified in a simulator Gazebo.

Using these models, two algorithms, aimed at the localization of a previously unknown source of radiation, were designed. One algorithm utilizes a single UAV equipped with one detector and the ability to determine direction of incomming particles. The purpose of this algorithm was to find a simple, low-cost solution to the problem. The other approach uses a formation of three, relatively localized UAVs, each equipped with its own detector. An Unscented Kalman filter (UKF) is used for state estimation in this non-linear system. The target final position of the formation is aimed to provide the maximal directional coverage and the most accurate estimation of the position of the source.

Both of the approaches have been thoroughly tested in the simulator Gazebo. Presented algorithm for solo localization encountered some obstacles which have been overcome during the testing. Based on the simulations, the solo approach provided the best results after three iterations. Additional iterations did not necessarily increased precision. Although this approach was not expected to perform very well, multiple simulations uncovered, that after three iterations the algorithm provides consistent results and an average estimation error under 2 meters. The largest drawback of this approach is its time consumption. Every iteration of the algorithm requires at least 2 additional minutes in the air.

The cooperative approach was aimed to provide a faster and more accurate solution. The UAVs move in a fixed formation over the whole defined area at maximum speed, creating a rough map of radiation intensity. This map is then used to initialize the UKF. Using this approach, the UAVs were able to find a fairly weak source of radiation on an area of 100×100 m under 5 minutes, with an error of only 50 centimeters.

In addition to the simulations, the localization algorithms were also tested with a real UAV platform. These experiments were also performed without a real radioactive material, which was replaced by the radiation model designed in this thesis. A sample of Cesium was simulated directly by the onboard computers of the UAVs. All of the real experiments were successful, closely resembling the behavior in simulations. The biggest difference can be seen in the radiation intensity maps, which are much more noisy in the real experiments. The sensors were not logging with a synchronized frequency, which introduced gaps into the final map, because the leader had to wait for measurements from the other two UAVs. Despite the noise, the algorithm performed exceptionally well, achieving a targetting error of only 1.6 meters.

Results of the simulations are presented in Section 6 and results of real experiments in Section 7. The best way to visualize these experiments, however, is in a video containing both real footage and animated plot of the measurements. Four videos are linked to this

work - a solo localization in simulator[1], a cooperative localization in simulator[2], a real experiment with one helicopter[3] and a real experiment with a formation of helicopters[4]. All these videos are also avaliable in on the CD attached to this thesis.

8.1 Future work

This thesis is a first step of a new research direction conducted at CTU in Prague, and more work in this field is expected. The most important part is to test the ability to detect a direction of incomming particles with a real detector. The entire localization process could also be improved by using a detector, which can already predict the direction, therefore eliminating the necessity to stop and rotate the UAV in one place. The radiation models were also designed with the ability to create a more complex enviroment with more than one source. This opens a way to solve even more difficult tasks. The entire research could ultimately result with a deployment in heavily irradiated areas, such as the Fukushima nuclear power plant in Japan.

Figure 37 A photo taken during the real experiment showing the three UAVs hovering above the position of a radiation source (represented by a white barrel).

[1]Simulation solo - `https://www.youtube.com/watch?v=x8hacOAcJlY`
[2]Simulation formation - `https://www.youtube.com/watch?v=6GEYo5El-zQ`
[3]Real solo - `https://www.youtube.com/watch?v=_KBGdi1a2do`
[4]Real formation - `https://www.youtube.com/watch?v=aZLEAHczIBw`

Bibliography

[1] D Turecek et al. “Pixelman: a multi-platform data acquisition and processing software package for Medipix2, Timepix and Medipix3 detectors”. In: *Journal of Instrumentation* 6.01 (2011), p. C01046.

[2] Zdeněk Vykydal. “Mikroprocesorem řízené rozhraní USB pro detektor Medipix2”. Master thesis. Faculty of Nuclear Sciences and Physical Engineering, Czech Technical University in Prague, 2005.

[3] Jan Jakubek. “Data processing and image reconstruction methods for pixel detectors”. In: *Nuclear Instruments and Methods in Physics Research Section A: Accelerators, Spectrometers, Detectors and Associated Equipment* 576.1 (2007), pp. 223–234.

[4] Michal Platkevič. “Signal Processing and Data Read-Out from Position Sensitive Pixel Detectors”. PhD thesis. Faculty of Nuclear Sciences and Physical Engineering, Czech Technical University in Prague, 2014.

[5] *Nuclear Security*. URL: `http://www.dhs.gov/topic/nuclear-security` (visited on 05/23/2017).

[6] *Gazebo - Robot simulation made easy*. URL: `http://gazebosim.org/` (visited on 04/24/2017).

[7] WB Atwood et al. “The Large Area Telescope on the Fermi gamma-ray space telescope mission”. In: *The Astrophysical Journal* 697.2 (2009), p. 1071.

[8] Carlos Granja et al. “The SATRAM Timepix spacecraft payload in open space on board the Proba-V satellite for wide range radiation monitoring in LEO orbit”. In: *Planetary and Space Science* 125 (2016), pp. 114–129.

[9] T Baca et al. “Miniaturized X-ray telescope for VZLUSAT-1 nanosatellite with Timepix detector”. In: *Journal of Instrumentation* 11.10 (2016), p. C10007.

[10] Lawrence S Pinsky et al. “Medipix in space on-board the ISS”. In: *Journal of radiation research* (2014).

[11] PG Martin et al. “Low altitude unmanned aerial vehicle for characterising remediation effectiveness following the FDNPP accident”. In: *Journal of environmental radioactivity* 151 (2016), pp. 58–63.

[12] JW MacFarlane et al. “Lightweight aerial vehicles for monitoring, assessment and mapping of radiation anomalies”. In: *Journal of environmental radioactivity* 136 (2014), pp. 127–130.

[13] Stuart M Adams and Carol J Friedland. *A survey of unmanned aerial vehicle (UAV) usage for imagery collection in disaster research and management*. publisher not identified, 2011.

[14] Roy Pöllänen et al. “Radiation surveillance using an unmanned aerial vehicle”. In: *Applied radiation and isotopes* 67.2 (2009), pp. 340–344.

[15] Jinlu Han et al. “Low-cost multi-UAV technologies for contour mapping of nuclear radiation field”. In: *Journal of Intelligent & Robotic Systems* (2013), pp. 1–10.

[16] *FlyCam*. URL: `http://www.flycamuav.com/aerial-radiation-detection/` (visited on 05/23/2017).

[17] Martin Saska et al. "Coordination and navigation of heterogeneous MAV–UGV formations localized by a 'hawk-eye'-like approach under a model predictive control scheme". In: *The International Journal of Robotics Research* 33.10 (2014), pp. 1393–1412.

[18] Martin Saska et al. "Fault-tolerant formation driving mechanism designed for heterogeneous MAVs-UGVs groups". In: *Journal of Intelligent & Robotic Systems* 73.1-4 (2014), p. 603.

[19] Vojtech Spurny, Tomas Baca, and Martin Saska. "Complex manoeuvres of heterogeneous MAV-UGV formations using a model predictive control". In: *Methods and Models in Automation and Robotics (MMAR), 2016 21st International Conference on*. IEEE. 2016, pp. 998–1003.

[20] Martin Saska, Zdenek Kasl, and Libor Přeucil. "Motion planning and control of formations of micro aerial vehicles". In: *IFAC Proceedings Volumes* 47.3 (2014), pp. 1228–1233.

[21] Martin Saska et al. "Navigation, localization and stabilization of formations of unmanned aerial and ground vehicles". In: *Unmanned Aircraft Systems (ICUAS), 2013 International Conference on*. IEEE. 2013, pp. 831–840.

[22] Martin Saska et al. "Coordination and navigation of heterogeneous UAVs-UGVs teams localized by a hawk-eye approach". In: *Intelligent Robots and Systems (IROS), 2012 IEEE/RSJ International Conference on*. IEEE. 2012, pp. 2166–2171.

[23] Martin Saska. "MAV-swarms: Unmanned aerial vehicles stabilized along a given path using onboard relative localization". In: *Unmanned Aircraft Systems (ICUAS), 2015 International Conference on*. IEEE. 2015, pp. 894–903.

[24] Martin Saska, Jan Vakula, and Libor Přeučil. "Swarms of micro aerial vehicles stabilized under a visual relative localization". In: *Robotics and Automation (ICRA), 2014 IEEE International Conference on*. IEEE. 2014, pp. 3570–3575.

[25] Matouš Vrba. "Active Searching of RFID Chips by a Group of Relatively Stabilized Helicopters". Bachelor thesis. Faculty of Electrical Engineering, Czech Technical University in Prague, 2016.

[26] Martin Saska et al. "Swarm distribution and deployment for cooperative surveillance by micro-aerial vehicles". In: *Journal of Intelligent & Robotic Systems* 84.1-4 (2016), pp. 469–492.

[27] Martin Saska et al. "System for deployment of groups of unmanned micro aerial vehicles in GPS-denied environments using onboard visual relative localization". In: *Autonomous Robots* (2016), pp. 1–26.

[28] Martin Saska et al. "Autonomous deployment of swarms of micro-aerial vehicles in cooperative surveillance". In: *Unmanned Aircraft Systems (ICUAS), 2014 International Conference on*. IEEE. 2014, pp. 584–595.

[29] K. Pine et al. "Radio direction finding for maritime search and rescue". In: *2004 5th Asian Control Conference (IEEE Cat. No.04EX904)*. Vol. 2. July 2004, 723–730 Vol.2.

[30] Martin Saska, Jan Langr, and Libor Přeučil. "Plume Tracking by a Self-stabilized Group of Micro Aerial Vehicles". In: *Modelling and Simulation for Autonomous Systems: First International Workshop, MESAS 2014, Rome, Italy, May 5-6, 2014, Revised Selected Papers*. Ed. by Jan Hodicky. Cham: Springer International Publishing, 2014, pp. 44–55. ISBN: 978-3-319-13823-7. DOI: 10.1007/978-3-319-13823-7_5. URL: http://dx.doi.org/10.1007/978-3-319-13823-7_5.

[31] Eric M Becker. "A Direction-Sensitive Radiation Detector for Low-Altitude, UAV-based Radiological Source Search". PhD thesis. School of Nuclear Science and Engineering, Oregon State University, 2015.

[32] Jan Faigl et al. "Low-cost embedded system for relative localization in robotic swarms". In: *Robotics and Automation (ICRA), 2013 IEEE International Conference on*. IEEE. 2013, pp. 993–998.

[33] Tomáš Krajn´k et al. "A practical multirobot localization system". In: *Journal of Intelligent & Robotic Systems* 76.3-4 (2014), pp. 539–562.

[34] Tomas Baca, Giuseppe Loianno, and Martin Saska. "Embedded model predictive control of unmanned micro aerial vehicles". In: *Methods and Models in Automation and Robotics (MMAR), 2016 21st International Conference on*. IEEE. 2016, pp. 992–997.

[35] Jan Jakůbek. *Pixel device TimePix*. URL: http://aladdin.utef.cvut.cz/ofat/others/Timepix/index.htm (visited on 04/30/2017).

[36] CERN collaboration. *The Timepix Chip*. URL: https://medipix.web.cern.ch/medipix/pages/medipix2/timepix.php (visited on 01/17/2017).

[37] Daniel Vavrik et al. "Advanced X-ray radiography and tomography in several engineering applications". In: *Nuclear Instruments and Methods in Physics Research* (2010).

[38] J Zemlicka et al. "Analysis of painted arts by energy sensitive radiographic techniques with the Pixel Detector Timepix". In: *Journal of Instrumentation* (2011).

[39] P Soukup, J Jakubek, and Z Vykydal. "3D sensitive voxel detector of ionizing radiation based on Timepix device". In: *Journal of Instrumentation* 6.1 (2011), p. C01060. URL: http://stacks.iop.org/1748-0221/6/i=01/a=C01060.

[40] *The Timepix Chip*. URL: http://wiki.ros.org/ (visited on 04/24/2017).

[41] G. Weber. *X-Ray attenuation absorption calculator*. URL: http://web-docs.gsi.de/~stoe_exp/web_programs/x_ray_absorption/index.php (visited on 01/26/2017).

[42] Eric A Wan and Rudolph Van Der Merwe. "The unscented Kalman filter for nonlinear estimation". In: *Adaptive Systems for Signal Processing, Communications, and Control Symposium 2000. AS-SPCC. The IEEE 2000*. Ieee. 2000, pp. 153–158.

[43] Antonio Giannitrapani et al. "Comparison of EKF and UKF for spacecraft localization via angle measurements". In: *IEEE Transactions on aerospace and electronic systems* 47.1 (2011), pp. 75–84.